Geosci. Model Dev., 19, 7217–7237, 2026
https://doi.org/10.5194/gmd-19-7217-2026

Geoscientific Model Development
Open Access

Resolving effects of leaf pigmentation changes and plant residue on the energy balance of winter wheat cultivation in the ORCHIDEE-CROP model

Ke Yu[1], Yang Su[1,2,3], Ronny Lauerwald[2], Philippe Ciais[1], Yi Xi[1], Haoran Xu[1], Xianglin Zhang[2], Nicolas Viovy[1], Amie Pickering[4], Marie Collard[5], and Daniel S. Goll[1]

[1]Laboratoire des Sciences du Climat et de l'Environnement, LSCE/IPSL, CEA-CNRS-UVSQ, Université Paris-Saclay, Gif-sur-Yvette, 91191, France
[2]UMR ECOSYS, INRAE AgroParisTech, Université Paris-Saclay, Palaiseau, 91120, France
[3]Département d'Informatique, École Normale Supérieure-PSL, Paris, 75005, France
[4]Game & Wildlife Conservation Trust (GWCT), The Allerton Project, Loddington, Leicestershire, UK
[5]Département durabilité, systèmes et prospectives, Centre wallon de Recherches agronomiques (CRA-W), 6800 Libramont, Belgium

Correspondence: Ke Yu (ke.yu@lsce.ipsl.fr) and Yang Su (yang.su@ens.fr)

Received: 23 April 2025 – Discussion started: 2 July 2025
Revised: 13 May 2026 – Accepted: 3 July 2026 – Published: 6 August 2026

Abstract. Crop management impacts climate not only through changes in carbon stocks and greenhouse gas budgets, but also through alterations in the surface energy budget. However, the latter aspect remains only partially represented in current cropping system models. Coupling dedicated crop models with land surface models provides a promising approach for quantifying these effects, but this effort is hindered by the simplistic representation of surface albedo as a combination of soil albedo and a static vegetation albedo controlled by vegetation cover. Here, we developed ORCHIDEE-CROP, a land surface model integrating the cropping system model STICS, by incorporating time-varying albedo from crop pigmentation during foliar yellowing and post-harvest crop residue soil cover. We further parameterized the effect of crop residues on surface roughness and soil evaporation affecting the surface energy budget and partitioning between latent and sensible heat fluxes. Using 10 site simulations, we quantified the impacts of these processes on soil temperature, soil moisture, water and heat fluxes of winter wheat crops. Incorporating foliar yellowing and post-harvest residue cover increased surface albedo by an average of 0.07 ± 0.03 during the foliar yellowing period and 0.02 ± 0.02 during the residue cover period, accordingly inducing surface cooling by -1.55 ± 0.93 and -1.90 ± 0.88 °C. During each period, sensible heat flux changed by -8.10 ± 4.18 and $-7.44 \pm 3.98\,\mathrm{W\,m^{-2}}$, while latent heat flux decreased by -6.84 ± 1.41 and $-5.15 \pm 4.03\,\mathrm{W\,m^{-2}}$. The spatiotemporal variability of these effects was driven by site-specific meteorology and soil properties. Simulations under dry scenarios reveal that crop residues left on the field can progressively increase plant-available water over multiple years under dry conditions. This study underscores that crop pigmentation has a minor influence on water–heat processes, while residues moderately modulate surface energy partitioning with significant spatial heterogeneity, highlighting the potential of residue management for climate mitigation. The refined modelling framework enables simultaneous assessment of the biogeochemical and biophysical impacts of field operations on the Earth System.

1 Introduction

Agriculture and climate are interconnected by greenhouse gas, energy and water budgets (IPCC, 2014; Wu et al., 2016; Chen et al., 2024). These interactions create a dual challenge that agricultural systems are both vulnerable to climate change impacts (e.g., droughts, extreme weather) and significant contributors to global emissions. Adaptive management practices are therefore critical for enhancing agricultural resilience and sustainability while simultaneously reducing anthropogenic disturbances to the environment and climate. To quantify the complex spatiotemporal climate impacts of management practices, coupling land surface models with dedicated crop modules represents a promising strategy. These models are effective tools for simulating biophysical and biogeochemical processes at the agriculture–climate interface, such as crop physiological growth, yield dynamics, and the exchange of carbon, water, and energy between agroecosystems and the atmosphere (Brisson et al., 2003; Fisher et al., 2014; McDermid et al., 2017). By capturing these processes, land surface models provide essential insights for projecting future climate-agriculture feedback under varying management scenarios (Arora et al., 2023; Timlin et al., 2024). However, a key limitation arises from the inconsistency between the diversity and complexity of real-world agricultural management practices and their overly simplistic representations in current land surface models. This gap significantly hinders the ability of land surface models to reliably predict climate impacts, particularly at regional or farm-specific scales where management decisions are highly required (Fisher and Koven, 2020). A key example of the limited ability of land surface models in representing biophysical processes of agriculture–climate interactions is their treatment of crop albedo dynamics.

Surface albedo, as the fraction of incoming solar radiation that is reflected by the soil and crops, plays a critical role in both radiative and non-radiative climate processes (Seneviratne et al., 2018; Zhang et al., 2022a). Crops and their residues exhibit distinct albedo due to differences in plant traits (e.g., leaf pigmentation, canopy structure) and management practices (e.g., tillage, residue retention, irrigation). For example, existing research shows an averaged albedo of 0.16–0.19 for winter wheat (Şerban et al., 2011; Sieber et al., 2022; Lei et al., 2024), of 0.18–0.20 for soybean (Costa et al., 2007; Lei et al., 2024), and of 0.15–0.18 for corn (Jacobs and van Pul, 1990; Lei et al., 2024). These differences in albedo directly affect global climate by changing the radiative forcing at the top of the atmosphere (Stephens et al., 2015). In addition, changes in surface albedo modify the surface energy balance, potentially redistributing energy between latent and sensible heat fluxes through non-radiative processes. However, land surface models generally use simplistic parameterizations of static soil and crop albedo. When temporal dynamics are included, they are typically limited to changes in the fractional coverage of soil and vegetation (Dalgliesh et al., 2016; Wu et al., 2016; Hoogenboom et al., 2024). Because they lack mechanisms to represent changes in crop pigmentation, these models are poorly suited to quantify climate effects of managements or crop breeding which affect crop residue or crop pigmentation (e.g., no tillage, pale crops) (Drewry et al., 2014).

Winter wheat, as a major cereal crop, undergoes distinct phenological stages that are accompanied by changes in canopy pigmentation and surface reflectance (Zhang et al., 2022b). During its growth cycle, winter wheat transitions from chlorophyll-dominated green leaves to senescent yellow leaves after maturity, where reduced chlorophyll levels expose light-reflecting carotenoids (Féret et al., 2017). Additionally, crop residues left on the field after harvest introduce additional albedo variability compared with bare soil in conventional tillage systems, with the extent of this fluctuation depending on the baseline bare soil albedo and residue management practices (Simão et al., 2021). Generally higher albedo of vegetation than bare soil in most croplands in Europe possibly induces an increase in surface albedo when covering residues on the soil (Pique et al., 2023). Such physiological development of winter wheat and residue coverage therefore affect the climate through changes in surface albedo, potentially offsetting part of the warming caused by greenhouse gas emissions. However, it is difficult for current land surface models to quantify and evaluate these effects because they are generally ignored or parameterized using simplified assumptions (Davin et al., 2014; Sieber et al., 2022; Yu et al., 2024).

This study simulates the biophysical impacts of winter wheat phenology and residue management on surface energy balance through albedo-mediated processes in the ORCHIDEE-CROP land surface model. To achieve this, we improved the model by refining the representation of foliar pigmentation and crop residue effects on albedo dynamics, as well as their influence on soil evaporation and surface roughness based on observations from 10 European cropland sites. Section 2 details the datasets and methodology used for model parameterization. We briefly review the baseline modeling representation of surface albedo, hydrology, roughness, and energy fluxes before introducing our modifications in ORCHIDEE-CROP. These improvements enhance the representation of albedo dynamics, soil evaporation, and surface roughness, with two simulations for evaluating the albedo-mediated impact of residue retention conducted under both current and dry scenarios. Section 3 presents the results of these refinements, while Sect. 4 analyses the contribution of albedo changes, driven by foliar pigmentation and crop residues, on modulating surface temperature, latent heat, and sensible heat fluxes. We also discuss the potential of crop residue management for climate adaptation and mitigation. Finally, Sect. 5 summarizes our findings and conclusions. By incorporating albedo dynamics influenced by crop pigmentation and residue management, this study enhances the realism of coupled cropland surface models and demonstrates its impacts on field-level energy balance under present and future idealised climate.

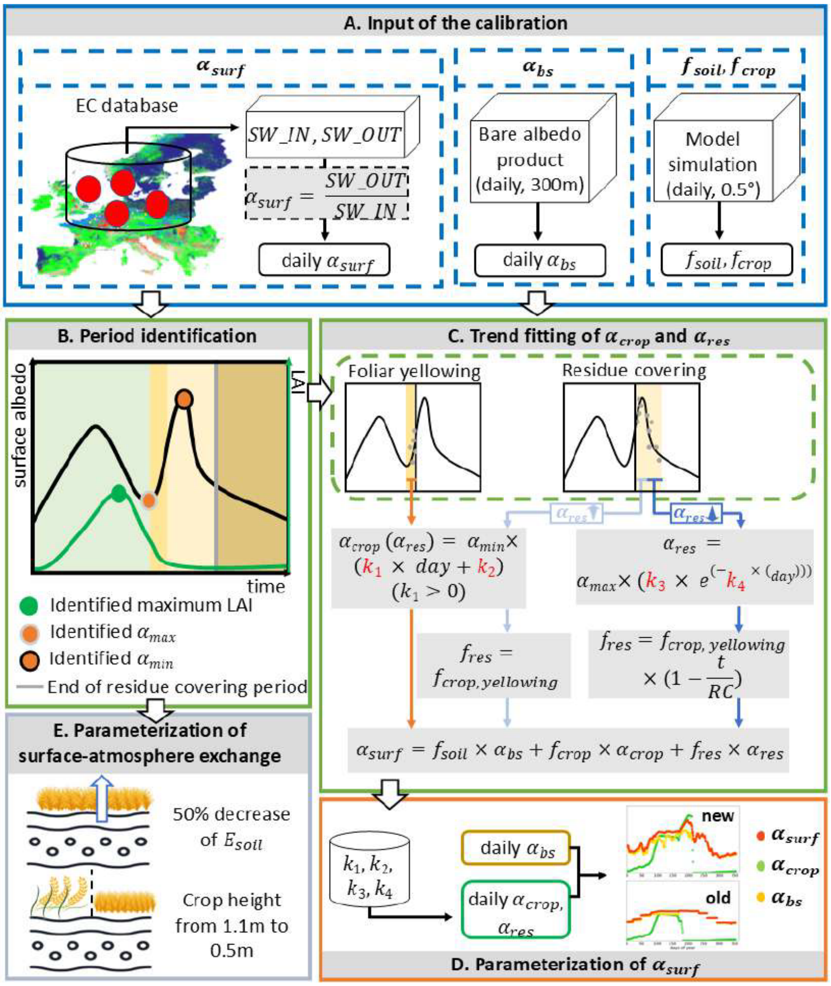

Figure 1. The procedure of parameterization of crop and residue albedo (α_{surf} and α_{res}), soil evaporation (E_{soil}) and surface roughness (Z_0) in the ORCHIDEE-CROP model. Panel **(A)** illustrates the input datasets for albedo calibration. α_{soil} and α_{surf} are bare soil albedo (α_{soil}) and surface albedo (α_{surf}), respectively. f_{crop} and f_{soil} are the gridded fractions of crop (f_{crop}) and residues (f_{res}), respectively. SW_IN and SW_OUT are half-hourly incoming (SW_IN) and outgoing (SW_OUT) solar radiance observed at seven eddy-covariance (EC) sites. Panel **(B)** shows the identification of foliar yellowing and residue covering periods based on time series of α_{surf} (black curve) and leaf area index (LAI, green curve). α_{min} and α_{max} are the identified minimum and maximum α_{surf}. The shallow-green, orange, yellow and brown areas show the conceptual growing, maturity, residue covering and bare soil periods of winter wheat. Panel **(C)** describes trend fittings for crop albedo (α_{crop}) and α_{res}. Features in two plots have the same meanings with the ones in Panel **(B)**. $f_{crop,yellowing}$ is the fraction of crop during the foliar yellowing period. RC is the duration of residue covering. k_1, k_2, k_3 and k_4 are the fitting parameters during foliar yellowing and residue covering periods. Day and t are the days of α_{surf} increase during residue covering period. Panel **(D)** illustrates parameterization of α_{surf} as a weighted combination of α_{crop}, α_{res} and α_{soil} in ORCHIDEE-CROP model. The daily α_{surf} in orange in the upper plot is derived from the new calibrated process based on k_1–k_4, compared to the old model (plot below). Panel **(E)** presents parameterization of surface–atmosphere exchange. E_{soil} is the soil evaporation and the dotted vertical line represents the harvesting date of winter wheat.

2 Data and methods

The improvements of the ORCHIDEE-CROP model are illustrated in Fig. 1 and structured into six subsections: (1) Datasets (Sect. 2.1); (2) Introduction of the ORCHIDEE-CROP model (Sect. 2.2); (3) New parameterization of the ORCHIDEE-CROP model (Sect. 2.3); (4) Model calibration (Sect. 2.4); (5) Model simulations (Sect. 2.5); (6) Model evaluation (Sect. 2.6).

2.1 Datasets

2.1.1 Daily surface albedo from site observation

To derive surface albedo (α_{surf}, unitless) from site observations, we combined datasets from two sources: (1) eddy-covariance measurements from the Integrated Carbon Observation System (ICOS) Data Portal (Dumont et al., 2024; Schmidt et al., 2025; Buysse et al., 2023; Brut et al., 2024;

Brümmer et al., 2023; Tallec et al., 2026; Bernhofer et al., 2026), and (2) satellite-derived products at farms belonging to the ClieNFarm project. From the ICOS network, we obtained the half-hourly incoming and outgoing solar radiance (SW_IN and SW_OUT, $\mathrm{W\,m^{-2}}$) measurements from 2000 to 2020 at eight wheat cultivated sites (BE-Lon, CH-Oe2, DE-Geb, DE-Kli, DE-RuS, FR-Aur, FR-Gri, FR-Lam) (Fig. S1 in the Supplement). Data were quality-controlled and gap-filled using uniform methods (Pastorello et al., 2020). Details of the quality filtering and preprocessing procedures of α_{surf} are provided in Sect. S1.1 in the Supplement. The daily short-wave mid-day α_{surf} was calculated from average values of SW_IN and SW_OUT from 11:00 to 13:00 Central European Summer Time at each site (Lin et al., 2023):

$$\alpha_{\mathrm{surf}} = \frac{\mathrm{SW\_OUT}}{\mathrm{SW\_IN}} \tag{1}$$

At six farms across two ClieNFarm sites (UK-Rookery, UK-Winwick, UK-Allerton, BE-AH, BE-BM, BE-LB) where direct radiation measurements were unavailable, we estimated surface albedo at 5 d intervals and 300 m resolution using Sentinel-2 (S2) reflectance data. A 10 % cloud-cover threshold was applied for quality filtering, and retrievals followed the framework developed by Lin et al. (2023). For the selected 10 sites, we chose only the years during which winter wheat was cultivated, and obtained a total of 33 winter wheat years.

2.1.2 Meteorological data from site observation

We utilized the half-hourly meteorological observations from flux towers in the winter wheat years at eight ICOS sites to force the ORCHIDEE-CROP model. The observations include SW_IN, surface pressure (Pa), near-surface specific humidity ($\mathrm{kg\,kg^{-1}}$), rainfall rate ($\mathrm{kg\,m^{-2}\,s}$), snowfall rate ($\mathrm{kg\,m^{-2}\,s}$), near-surface air temperature (K), and near-surface eastward and northward wind components ($\mathrm{m\,s^{-1}}$). The FLUXNET_DATA tool (available upon request from the authors) was used to fill gaps in the flux-towers data using 6-hourly ERA-interim products (Vuichard and Papale, 2015). We then averaged all gap-filled variables to a 6 h time step to meet the input requirements of the model. At the two ClieNFarm sites without flux observations, the meteorological variables from the hourly 0.25° ERA-interim product were extracted and interpolated to exact site coordinates to provide meteorological forcing data.

In 10-year simulations for the current climate scenario from 2010 to 2020 (Sect. 2.5), the processed climate forcing data from each year obtained from the ICOS Data Portal was used to drive the model. For the dry scenario, the driest year at each site was identified based on the lowest annual precipitation. All meteorological variables from this year were then used to force the simulation. This approach ensures that the dry scenario is driven by a coherent and physically realistic set of meteorological conditions. Yearly-averaged meteorological variables in the driest year for each site are presented in Table S1 in the Supplement.

2.1.3 Management practice, bare soil albedo and LAI

Management practices during the winter wheat cultivation year at all sites (Table S2 in the Supplement) were obtained from a crop management database provided by site managers. Key practices, including sowing, harvesting, and tillage dates, were prepared as input for the ORCHIDEE-CROP model.

Bare soil albedo (α_{soil}, unitless) was prescribed using a high-resolution 5 d, 300 m European α_{soil} dataset derived from 10 m S2-α_{surf} observations covering the period 2018–2020 (Yu et al., 2026). This dataset demonstrated sufficient skill in resolving daily soil dynamics at the field scale in fragmented European croplands. Since the model was run at the site scale, bare soil albedo values were extracted for each site location, and linear interpolation was applied to convert the data to a daily time step, aligned with the model temporal resolution.

Due to the absence of sporadic leaf area index (LAI, $\mathrm{m^2\,m^{-2}}$) measurements found at ICOS sites (Table S3 in the Supplement), we used continuous satellite-based LAI datasets to identify the timing of peak LAI at those sites. LAI at each site was extracted from the 4 d, 500 m LAI product from the MODIS (MCD15A3H) (Myneni et al., 2015). Daily LAI dynamics were derived through linear interpolation combined with a Savitzky–Golay filter (window length = 15) to smooth the trend and remove the outliers. MODIS-derived LAI was used to constrain the onset of crop maturity period, rather than to reproduce absolute LAI values. The LAI comparison between MODIS product and site measurements is shown in Fig. S2 in the Supplement. We used the MODIS-derived LAI product rather than the S2-derived product, because the temporal coverage of the latter is insufficient to match the available site observations.

2.2 Introduction of the ORCHIDEE-CROP model

The ORCHIDEE-CROP model is a branched version of the process-based land surface model, ORCHIDEE (Krinner et al., 2005), which incorporates a generic crop phenology and harvest module, along with simplified nitrogen fertilization parameterization based on the process-based STICS formalism (Wu et al., 2016). It simulates biophysical and biogeochemical interactions in croplands, as well as plant productivity and harvested yield. A detailed model description is available in Wu et al. (2016). This study employs a previously developed model version calibrated against LAI, flowering and harvesting dates, and crop yield for both winter wheat and maize (https://github.com/yangsssu/ORCHIDEE-CROP.git, last access: 13 February 2026). In the present study, only winter wheat is considered. The derived climate and management information were used to drive the model as forcing data (Sect. 2.1.2 and 2.1.3). Winter wheat is the only vegetation type considered in this analysis. To assess the impacts of winter wheat physiological development and residue coverage on the surface energy balance and water–energy fluxes, we describe below the key processes governing surface energy balance (Sect. 2.2.1), α_{surf} dynamics (Sect. 2.2.2), hydrology (Sect. 2.2.3), the surface roughness (Sect. 2.2.4), as well as crop growth and development (Sect. 2.2.5).

2.2.1 Surface energy balance

The ORCHIDEE-CROP model simulates the surface energy budget by:

$$R_n = LE + H + G \tag{2}$$

where the net radiation (R_n, $\mathrm{W\,m^{-2}}$) governs land–atmosphere water and heat exchange, driven by the partitioning of *LE*, sensible heat fluxes (H, $\mathrm{W\,m^{-2}}$) and soil heat fluxes (G, $\mathrm{W\,m^{-2}}$). R_n is determined by the net short-wave radiation budget (S_n, $\mathrm{W\,m^{-2}}$) and the net long-wave radiation budget (L_n, $\mathrm{W\,m^{-2}}$) (Ducoudré et al., 1993).

$$R_n = S_n + L_n = (1 - \alpha_{surf}) \times \mathrm{SW\_IN} + L\downarrow - L\uparrow \tag{3}$$

where $L\downarrow$ is the down-welling longwave radiation (a model input variable). $L\uparrow$ is the upwelling longwave radiation emitted by the land surface, which is estimated by surface temperature (T_{surf}, K) (a model input variable) based on Stefan–Boltzmann law.

Because α_{surf} directly influences R_n, its formulation in the ORCHIDEE-CROP model is described below.

2.2.2 Surface albedo dynamics

The model calculates α_{surf} in step t for both the visible and near-infrared domains by the area-weighted sum of foliar albedo (α_{crop}, unitless) and α_{soil}:

$$\alpha_{surf}(t) = (1 - f_{crop}(t)) \times \alpha_{soil}(t) + f_{crop}(t) \times \alpha_{crop,constant} \tag{4}$$

where $f_{crop}(t)$ and $1 - f_{crop}(t)$ represent the fractions of winter wheat and bare soil covering the surface area of the model pixel; $\alpha_{crop,constant}$ of winter wheat is set as the default value of 0.1 and 0.3 for visible and near-infrared ranges of α_{crop}, respectively. $\alpha_{soil}(t)$ is derived from daily α_{soil} dataset (Sect. 2.1.3). Since α_{surf} affects radiation absorption, it influences soil moisture availability and, consequently, soil evaporation (E_{soil}).

2.2.3 Hydrology

The ORCHIDEE-CROP model computes soil water budget by considering the three reservoirs of canopy interception, snow packing and 11 soil layers (MacBean et al., 2020). The water fluxes at soil surface include water inputs from throughfall, snowmelt and irrigation, and water output from soil by surface runoff, bare soil evaporation and drainage. Here, we mainly describe the calculation of E_{soil} and the soil water content (SWC, $\mathrm{kg\,m^{-2}}$) in different soil layers.

The ORCHIDEE-CROP model calculates *LE* by accounting for snow sublimation, canopy interception and transpiration, E_{soil} and floodplain evaporation. A β-model is used to compute E_{soil} by inducing a series of aerodynamic and surface resistances.

$$\begin{aligned} E_{soil}(t) = {} & (1-\beta_1) \times (1-\beta_5) \times \beta_4 \times r_{au} \times v \times C_d \\ & \times (q_{surf} - q_{air}) \times \mathrm{d}t \end{aligned} \tag{5}$$

where β_1, β_4 and β_5 are dimensionless scaling factors representing soil moisture and surface resistance effects for snow sublimation (β_1), soil evaporation (β_4) and floodplain evaporation (β_5), respectively; r_{au} ($\mathrm{kg\,m^{-3}}$), v ($\mathrm{m\,s^{-1}}$), C_d (–), q_{surf} ($\mathrm{kg\,kg^{-1}}$), and q_{air} ($\mathrm{kg\,kg^{-1}}$) are the air density, wind speed, drag coefficient, saturated surface air moisture, and specific humidity, respectively. The bulk formulation yields evaporation in $\mathrm{kg\,m^{-2}\,s^{-1}}$, which is integrated over the model time step ($\mathrm{d}t$) to obtain values in $\mathrm{kg\,m^{-2}}$. This quantity is then expressed in $\mathrm{mm\,d^{-1}}$ using the equivalence $1\,\mathrm{mm} = 1\,\mathrm{kg\,m^{-2}}$.

Soil moisture dynamics are governed by a diffusive multi-layer soil hydrology scheme with 27 soil layers (up to 2 m), based on moisture diffusion principles (Richards, 1931; de Rosnay et al., 2002; Wu et al., 2016). It uses the 1D Richards equation with soil volumetric water content as the state variable in its saturated form, instead of the pressure head (Campoy et al., 2013).

2.2.4 Surface roughness

Surface roughness (Z_0, m) plays a critical role in regulating near-surface turbulence and the water–heat exchange process between the land surface and the atmosphere (Meier et al., 2022; Chen et al., 2024). E_{soil} depends on Z_0, which modulates atmospheric turbulence and moisture transfer. The ORCHIDEE-CROP model uses the averaged drag coefficients for momentum and heat transfer over winter wheat to compute the grid-averaged roughness height.

$$Z_0(t) = f_{crop}(t) \times \left(\frac{C_k}{\left(\frac{Z_{tmp}}{\max(H_c \times Z_{0,h},\, Z_{0,bare})} \right)} \right)^2 \tag{6}$$

where $Z_0(t)$ is the daily roughness height over each grid cell. C_k (–) is the von Karman constant, which equals to 0.41. Z_{tmp} (m) represents the maximum height of the first atmospheric layer and is determined by air pressure, air temperature, and air density. This variable represents the reference height used for flux calculations and is set to a minimum of 10 m above the ground. This ensures that the reference height remains above the canopy height, thereby maintaining the stability of the logarithmic function used in flux calculations. H_c (m) represents winter wheat height, which is treated as a time-invariant constant and set to 1.1 m in the ORCHIDEE-CROP model. For comparison, the maximum H_c of winter wheat during growing seasons measured at five sites has an average of 0.97 m (Table S3). $Z_{0,h}$ equals to 1/16, which is utilized to estimate the roughness height above the canopy. $Z_{0,bare}$ (m) is set as 0.01 m for roughness length of bare soil. Z_0 for the bare soil can be derived by:

$$Z_0(t) = (1 - f_{crop}(t)) \times \left(\frac{C_k}{\left(\frac{Z_{tmp}}{Z_{0,bare}} \right)} \right)^2 \quad (7)$$

The ORCHIDEE-CROP model computes a grid effective roughness height (H_{rough}, m) for deriving water–heat fluxes. It combines the zero-plane displacement height (Z_{dis}, m) which is an equivalent height for the absorption of momentum, and the vegetation height weighted by the maximum f_{crop} ($f_{crop,max}$) of winter wheat within each grid (H_{ave}, m):

$$H_{rough} = H_{ave} - Z_{dis} \quad (8)$$

$$Z_{dis} = H_{ave} \times H_{dis} \quad (9)$$

$$H_{ave} = f_{crop,max} \times H_c \quad (10)$$

H_{dis} (m) is used to determine the Z_{dis} based on H_{ave}, which equals to 0.75.

2.2.5 Crop growth and development

Crop development in the ORCHIDEE-CROP model is based on the crop model STICS (Wu et al., 2016). For winter wheat, the crop module simulates nine developmental stages of crop growth and grain filling (Fig. 2.1 in Brisson et al., 2003). The timing and duration of each developmental stage are calculated based on growing degree days adjusted by limiting functions related to photoperiod, vernalization and environmental constraints (e.g., water and nitrogen). Transitions between stages occur when the threshold values of growing degree days are reached.

In our simulations, sowing dates were prescribed using observed, site-specific management information to ensure consistency with field observations. Subsequent phenological development, including flowering, maturity, and harvest, is driven by growing degree days following the ORCHIDEE-CROP phenology scheme which was calibrated using extensive wheat phenology records from 1941 DWD climate stations across Germany (Su et al., 2025). This approach ensures that modeled flowering and harvesting dates are on average, consistent with observed phenology across a wide range of environmental conditions. We further adjusted the delay between crop maturation and harvest at each site using observed harvest dates which vary depending on management practices and weather conditions (Table S2).

2.3 New parameterization of the ORCHIDEE-CROP model

Foliar yellowing of winter wheat after maturation and crop residues remaining on the field after harvest affect α_{surf} and turbulent fluxes, but these processes are not currently represented in the model. As such, the absence of these key processes presents a gap in understanding and modeling of the impacts of winter wheat on regional energy and water cycles. We enhanced the ORCHIDEE-CROP model by introducing empirical functions describing temporal dynamics of α_{surf}, β_4 and Z_0 as a function of time, f_{crop} and f_{res} for foliar yellowing and crop residues. In addition, to ensure consistency between simulated and observed crop development periods (from sowing to harvest) at each site, the duration between maturity and harvesting in ORCHIDEE-CROP was calibrated using recorded harvesting dates at each site. In each winter wheat year at each site, simulations were performed iteratively with potential maturity-harvest intervals ranging from 5 to 40 d at 2 d increments. The optimal duration for each case was identified when the simulated harvest date matched the recorded management date. The calibrated durations are summarized in Table S2. It means that the site-specific durations of foliar yellowing before harvesting vary across all sites in the new model, compared to the default 14 d in the old model.

The objective of this model development targets a realistic mean effect size expected among European croplands, rather than capturing in detail the site-specific effects. We focus on improving the representation of albedo properties of winter wheat during the foliar yellowing and residue covering period, while associated impacts on surface energy fluxes are evaluated qualitatively rather than through a full recalibration of the hydrological scheme.

2.3.1 Improving albedo dynamics during the foliar yellowing periods

The foliar yellowing period in this model is defined as starting from the maturity date (nmat) and ending on the harvesting date based on analysis of observed α_{surf} dynamics at 10 sites (Sect. 2.4.1).

We replaced Eq. (4) with an equation which uses time-varying $\alpha_{crop}(t)$ instead of a $\alpha_{crop,constant}$:

$$\alpha_{surf}(t) = (1 - f_{crop}(t)) \times \alpha_{soil}(t) + f_{crop}(t) \times \alpha_{crop}(t) \quad (11)$$

To simulate the increase in α_{crop} after maturation and before harvesting we chose the following function:

$$\alpha_{crop}(t) = \alpha_{yellowing,start} \times (k_1 \times t + k_2) \quad (12)$$

Where $\alpha_{yellowing,start}$ is the simulated α_{crop} on the first day during the foliar yellowing period. k_1 and k_2 represent the fitting parameters that are calibrated at the multi-site scale (see below).

Here, we assumed that f_{crop} remains constant during the foliar yellowing periods ($f_{crop,yellowing}$).

2.3.2 Improving albedo dynamics during the residue covering periods

The residue covering period starts from the harvesting date and ends either 90 d after harvesting, or earlier if tillage occurs (Sect. 2.4.1). As α_{surf} continuously increases after harvesting due to the presence of light-colored and evenly distributed straws, we used the segmentation function to describe α_{surf} dynamics from increase and subsequent decrease in α_{surf} during this period.

The α_{surf} at each time step can be represented by the area-weighted sum of α_{soil} and α_{res}:

$$\alpha_{surf}(t) = (1 - f_{res}(t)) \times \alpha_{soil}(t) + f_{res}(t) \times \alpha_{res}(t) \tag{13}$$

$$\begin{cases} \alpha_{res}(t) = \alpha_{yellowing,start} \times (k_1 \times t + k_2) & t \text{ in albedo increase phase;} \\ \alpha_{res}(t) = \alpha_{max} \times \left(k_3 \times e^{-k_4 \times t}\right) & t \text{ in albedo decrease phase;} \\ \alpha_{res}(t) = 0 & \text{otherwise;} \end{cases} \tag{14}$$

Where α_{max} is the simulated α_{crop} on the last day of the albedo increase phase. $(1 - f_{res}(t))$ represent the daily variation of bare soil fraction. k_3 and k_4 represent the fitting parameters that need to be calibrated at the site scale (see below).

Here, f_{res} during the albedo increase phase equals to $f_{crop,yellowing}$ and linearly decreases during the albedo decrease stage from $f_{crop,yellowing}$:

$$\begin{cases} \{f_{res}(t) = f_{crop,yellowing} & t \text{ in albedo increase phase;} \\ f_{res}(t) = f_{crop,yellowing} \times \left(1 - \frac{t}{RC}\right) & t \text{ in albedo decrease phase;} \\ f_{res}(t) = 0 & \text{otherwise;} \end{cases} \tag{15}$$

RC is the maximum residue covering period, either equals to 90 d or the tillage date.

2.3.3 Considering the impact of crop residue on soil evaporation during the residue covering periods

Crop residues covering part of soil surface decrease E_{soil} by increasing the soil-to-atmosphere resistance (Horton et al., 1996). The current ORCHIDEE-CROP model does not consider the impact of crop residue on E_{soil}. Previous site-scale observations generally show a 20 %–50 % reduction in E_{soil} in the presence of wheat residue compared with bare soil (Unger and Parker, 1968; Lascano and Baumhardt, 1996; Ramos et al., 2024). Based on Eq. (5), we assumed a maximum initial reduction in soil conductance (β_4, unitless) of 50 % under the highest f_{res} (Zhao et al., 2020; Raes et al., 2022), with a progressive increase of conductance as daily f_{res} declines during the residue cover period:

$$\begin{aligned} E_{soil}(t) = {} & (1 - \beta_1(t)) \times (1 - \beta_5(t)) \times (1–0.5 \\ & \times f_{res}(t)) \times \beta_4(t) \times r_{au}(t) \times v(t) \times C_d(t) \\ & \times (q_{surf}(t) - q_{air}(t)) \times dt \end{aligned} \tag{16}$$

The meanings of all variables are the same as the ones in Eq. (5).

Note that β_4 represents an empirical resistance factor and cannot be directly inferred from observations. Therefore, its value was constrained through sensitivity testing against published experimental reductions in E_{soil} rather than calibrated directly using site-level flux measurements (Fig. S3 in the Supplement, Table S4 in the Supplement).

2.3.4 Considering the impact of crop residue on surface roughness during the residue covering periods

The initial version of the ORCHIDEE-CROP model assumed that Z_0 after harvest equals to that of bare soil coverage, omitting that (parts of the) stalks remain. To represent the impact of crop residues on Z_0 during the residue covering periods, we assumed that the H_c of plant changes from 1.1 m for winter wheat to 0.5 m for crop residues which has been identified as an optimal cutting height for harvest efficiency and soil and water conservation (MacMaster et al., 2000). f_{crop} is replaced with f_{res}. The new Z_0 and H_{rough} are therefore computed by:

$$Z_0(t) = f_{res}(t) \times \left(\frac{C_k}{\left(\frac{Z_{tmp}}{\max(0.5 \times Z_{0,h}, Z_{0,bare})}\right)} \right)^2 \tag{17}$$

$$H_{rough} = f_{crop,max} \times 0.5 - f_{crop,max} \times 0.5 \times H_{dis} \tag{18}$$

These two formulations remain identical to Eqs. (7) and (8), but with adjusted parameter values for canopy height and fractional cover to represent crop residues.

2.4 Model calibration

The parameters of α_{surf} dynamics were calibrated using data from 10 sites with 33 winter wheat site-years. α_{surf} and LAI observations were applied to identify foliar yellowing and residue covering periods at the available sites (Table S2).

2.4.1 Identifying the periods of foliar yellowing and residue covering from site observation

At the site scale, we assumed that foliar yellowing (i.e., α_{surf} increase) begins at crop maturity because no observational evidence supports a temporal gap between these two phases.

In the model, α_{surf} starts to increase after a delay following the maximum LAI and decreases after harvest. Post-harvest α_{surf} dynamics were divided into two phases: (1) an initial α_{surf} increase driven by light-colored, evenly distributed straw, followed by (2) a α_{surf} decline due to the dominating effects of decomposition of residues.

α_{surf} dynamics were parameterized by identifying critical temporal thresholds. The minimum α_{surf} between the LAI peak and harvest was used to define the onset of foliar yellowing, which is approximately 22.3 d (95 % bootstrap CI: [20.6–23.6] d, $n = 33$) pre-harvest computed by site observation. This delay is longer than the default 14 d interval between maturity and harvest used in the old ORCHIDEE-CROP model. The maximum α_{surf}, constrained to occur within 30 d after harvest, divided residue-driven α_{surf} dynamics into an increasing phase (harvest to maximum α_{surf}) and a decline phase from post-maximum α_{surf} to tillage. Without tillage, the residue covering period was assumed to persist for 90 d after harvest (Kriaučiūnienė et al., 2012). On average, the maximum α_{surf} occurs 13.4 d (95 % bootstrap CI: [10.5–15.9] d, $n = 33$) after harvest based on site identification, while the configuration in the old ORCHIDEE-CROP model does not consider the timing of maximum α_{surf}. Due to the lacking information of maximum α_{surf} during residue covering period in the old model, we utilized 15 d after harvesting as the boundary of these two phases in the ORCHIDEE-CROP model at all sites for simplification.

2.4.2 Parameter optimization of albedo dynamics

Daily α_{surf} and α_{soil} observations, together with information on bare soil exposure, were utilized to calibrate the empirical parameters k_1, k_2, k_3 and k_4 for α_{crop} and α_{res} (Eqs. 12 and 14). The $\alpha_{yellowing,start}$ (Eq. 12) was replaced by the α_{surf} observation at the beginning of the foliar yellowing period. The simulated f_{crop} from the old model and the calculated f_{res} (Eq. 13) were used because observations of fractional-cover changes were unavailable.

Data collected from 10 sites with 28 winter wheat years ($n = 485$ daily α_{surf} observation) were used to calibrate k_1, k_2, k_3 and k_4 in Eqs. (12) and (14). Data from the remaining five winter wheat years ($n = 179$ daily α_{surf} observation) were used for model testing. Finally, calibrated k_1, k_2, k_3 and k_4 were incorporated into the ORCHIDEE-CROP model to simulate the albedo dynamics affected by foliar yellowing and residue covering for all 10 sites.

2.5 Model simulations

Simulations were performed for 10 sites encompassing 14 farms (Table S2) with the new ORCHIDEE-CROP model version and with the original version of this model (Table 1) for the years for which observations were available. The experiments aimed to evaluate the impacts of the parameterizations of α_{surf}, β_4 and Z_0 on water–energy cycles during the foliar yellowing and residue covering periods. In the following, ORC-D refers to the default ORCHIDEE-CROP model configuration prior to any modifications, where "D" denotes the default setup. To assess the respective impacts of the five model modifications, we used five different configurations of the improved model. Configuration ORC-AE includes modifications to α_{surf}, β_4 and Z_0 during foliar yellowing and residue covering periods, where "A" refers to surface albedo and "E" to energy-related parameters. Configuration ORC-A includes only the modified α_{surf}, while ORC-E incorporates adjustments to both β_4 and Z_0. To further disentangle the individual impacts of β_4 and Z_0, ORC-Z_0 modifies only the Z_0, and ORC-β_4 refers to only the modification of the β_4. The prepared climate forcing data (Sect. 2.1.2), soil texture (sand, silt and clay contents) and crop management information (i.e., sowing date, tillage date, residue covering periods) (Sect. 2.1.3) for each site were used to drive the model. Note that all other management practices prescribed in this model (e.g., nitrogen fertilization) were set as default due to the lack of historical implementation records. There is no irrigation consideration in this analysis.

In addition, we conducted a 10-year simulation (2010–2020) under both current and idealised dry scenarios to quantify the cumulative effects of residue soil cover on water and heat fluxes for the new and old models at six sites if 10-year climate forcing data is available (Table S2). The meteorological forcing data for both scenarios followed the methodology described in Sect. 2.1.2, where the current climate scenario used observed annual climate data from ICOS, and the dry scenario was driven by climate forcing from the driest year (defined as the year with the lowest annual rainfall). The meteorological forcing from the driest year was repeated throughout the simulation period to represent persistent dry conditions. At each site, the sowing and harvesting dates were averaged across the years for which observations were available. The residue covering periods were assumed to persist for 60 d following winter wheat harvest in each year.

2.6 Sensitivity analysis

We performed sensitivity analyses of the major parameters (i.e. k_1, k_4, β_4, H_c, duration of α_{surf} increase during residue covering period (D_{up})) linking to the α_{surf} variation and the responses of the energy and water budgets, particularly for the ones without enough constraints from field observations. The sensitivity analysis was conducted by changing the parameters by ±10 %, ±20 % and ±30 % from the initial calibrated values. Their impacts of these parameter changes on T_{surf}, H, E_{soil} and LE were evaluated.

2.7 Model evaluation

We evaluated the performance of ORCHIDEE-CROP with and without modification against observations of α_{surf} at site

Table 1. Overview of simulation experiments and model configurations.

Names of experiments	Periods	Surface albedo	Parameter of soil conductance	Surface roughness	Crop and residue fraction	Test purpose
ORC-D		–	–	–	–	Control simulation
ORC-AE	Foliar yellowing	√	–	–	√	Combined impacts of surface albedo, soil resistance and surface roughness
	Residue covering	√	√	√	√	
ORC-A	Foliar yellowing	√	–	–	√	Isolated impact of surface albedo
	Residue covering	√	–	–	√	
ORC-E	Foliar yellowing	–	–	–	√	Combined impact of soil resistance and surface roughness
	Residue covering	–	√	√	√	
ORC-β_4	Foliar yellowing	–	–	–	√	Isolated impact of soil resistance
	Residue covering	–	√	–	√	
ORC-Z_0	Foliar yellowing	–	–	–	√	Isolated impact of surface roughness
	Residue covering	–	–	√	√	

"–" means there is no change, whereas "√" denotes that the corresponding parameter is modified relative to ORC-D. Note that the temporal evolution of foliar and residue albedo, soil resistance parameter, surface roughness, as well as changes in crop and residue fractions, follows the parameterizations described in Sect. 2.3, unless stated otherwise.

scale. The sites used for evaluation were independent from the ones used for calibration of α_{surf}.

We computed the coefficient of determination (R^2) and RMSE as quality indicators of model performance in the simulation-observation comparison of α_{surf} during the site calibration and model simulation processes (Wright, 1921; Carbone and Armstrong, 1982):

$$R^2 = 1 - \frac{\sum_i^n (y_i - f_i)^2}{\sum_i^n (y_i - \underline{y})^2} \tag{19}$$

$$\mathrm{RMSE} = \sqrt{\sum_i^n \frac{(f_i - y_i)^2}{n}} \tag{20}$$

Where n and i are the number of data and the data i in n in dataset; y_i and f_i are the value of observed data i and the value of fitted data i; $\underline{y}$ is the mean of the observed data.

With the calibration of the simulation of harvesting date for all sites, we further compared the simulated surface temperature (T_{surf}), LE, H from the old and new models against observation during the foliar yellowing and residue covering periods. For each variable, a paired t test was also used to assess the null hypothesis that the mean paired difference between the simulations from the old and new models differed significantly from zero.

3 Results

3.1 Evaluation of surface albedo dynamics in the refined ORCHIDEE-CROP model

During the albedo calibration phase, the estimated parameter values of k_1, k_2, k_3 and k_4 (Eqs. 12 and 14) are 0.013 (95 % CI: 0.012–0.013), 1.005 (95 % CI: 0.998–1.017), 0.895 (95 % CI: 0.889–0.902) and 0.0022 (95 % CI: 0.0017–0.0026), respectively. Using these calibrated parameters, the relationship between observed surface albedo (α_{surf}) and the parameterized α_{surf} representation used to constrain the model shows a moderate correlation with an R^2 of 0.54 during the foliar yellowing period and of 0.62 during the residue covering period for five testing sites. The corresponding RMSE values are 0.04 and 0.03, respectively (Fig. 2). The least-squares regression in these two fitting models captures the overall trend in the data better than models that consider them constant, but falls short of reproducing full variation, as it minimizes average errors rather than explaining outliers.

The refined ORCHIDEE-CROP configuration (ORC-AE), represents the new model version incorporating the modified α_{surf} together with the refined soil conductance (β_4) and surface roughness (Z_0) parameterizations, was used to simulate α_{surf} dynamics at all 33 site years, which were evaluated independently against observations (Fig. S4a and b in the Supplement). This independent evaluation demonstrates substantially stronger agreement, with significantly higher Pearson correlation coefficients compared to the default model configuration (ORC-D).

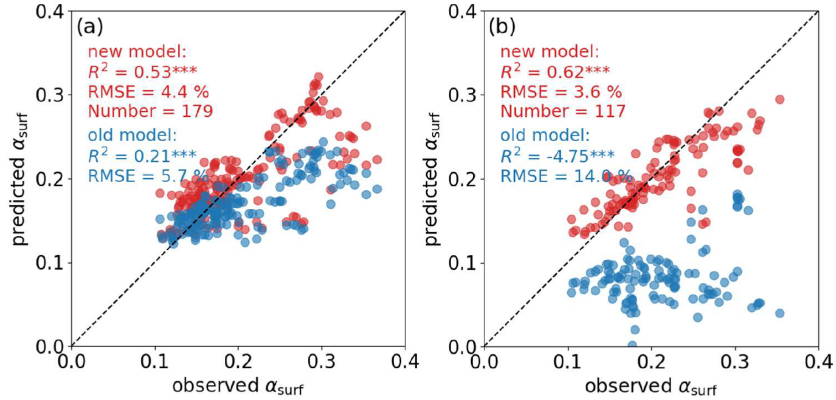

Figure 2. The comparison of daily surface albedo (α_{surf}) predictions derived from calibration models with and without explicit albedo parameterizations against independent observation from five sites in Europe during **(a)** the foliar yellowing and **(b)** residue covering periods. Coefficient of determination (R^2) and root mean square error (RMSE) are shown in the upper-left corners of each panel. "***" shows the comparison passes the significance level of 0.01. The dotted black line is the 1 : 1 line.

ORC-AE captured observed α_{surf} evolution during the foliar yellowing and residue covering periods across all five sites. Using FR-Gri as an example (Fig. 3), ORC-D without considering their effects on α_{surf} dynamics shows substantial biases in α_{surf} during the same period. The results of α_{surf} at all five sites are presented in Fig. S5 in the Supplement. α_{surf} increases during spring as crops LAI develops due to the enhanced reflected solar radiation of leaves compared to darker soil followed by a stable period before crops reach maturity. After the crop has reached maturity, the yellowing of aboveground crop biomass increases α_{surf}. This increase is reversed after harvest as dead and senescent plant material (i.e., residues) starts decomposing. Although the refined model can describe α_{surf} trends in both foliar yellowing and residue covering periods, substantial biases in α_{surf} remain for other periods which were not addressed in this study. These discrepancies result from inaccuracies of estimating bare soil albedo (Yu et al., 2026), from the growth of weeds which are not resolved in ORCHIDEE-CROP, and from the simplistic representation of vegetation albedo dynamics before maturity is reached.

3.2 The impact of improved surface albedo, surface roughness and soil conductance on soil evaporation, surface temperature and soil water content

Compared with the standard version of ORCHIDEE-CROP (ORC-D), statistically significant changes in averaged surface temperature (T_{surf}) are detected across sites in ORC-AE and ORC-E ($p < 0.05$ in t test), resulting from modifications in surface albedo (α_{surf}), surface roughness (Z_0), and soil conductance (β_4) (Table S5 in the Supplement). In contrast, modifying albedo alone (ORC-A) does not lead to statistically significant changes in soil evaporation (E_{soil}) during the foliar yellowing period ($p > 0.05$). Soil water content (SWC) generally does not exhibit statistically significant changes

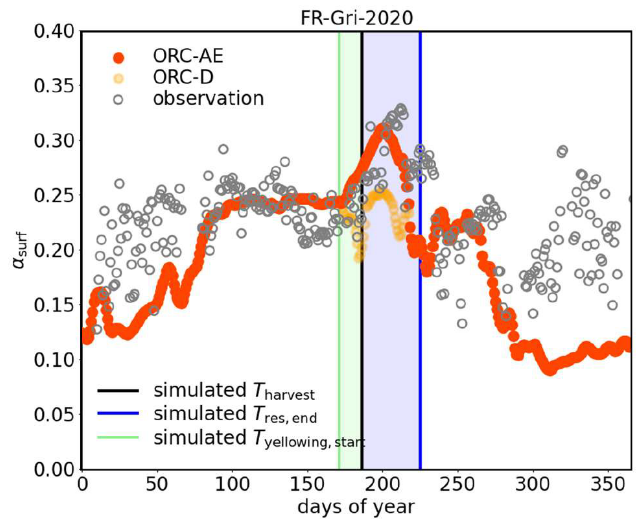

Figure 3. The comparison of surface albedo (α_{surf}) predicted from the old (orange dots, ORC-AE) and new (red dots, ORC-D) ORCHIDEE-CROP models and observations at Grignon site in France (gray dots) in 2020. ORC-AE represents the new model version with effects of the modified α_{surf} and the refined soil conductance (β_4) and surface roughness (Z_0), while ORC-D suggests the initial version of the model. The observed α_{surf} is computed from site radiation measurements through the Integrated Carbon Observation System (ICOS) Data Portal. The green, black and blue solid lines are the simulated start of the foliar yellowing period (shallow green area) ($T_{\mathrm{yellowing,start}}$), harvesting date ($T_{\mathrm{harvest}}$) and the end of residue covering period (shallow blue area) ($T_{\mathrm{res,end}}$), respectively.

($p > 0.05$) in any of the three model configurations. This indicates that, except for SWC, site-averaged differences in the targeted variables are detectable and exhibit consistent signs and magnitudes across sites.

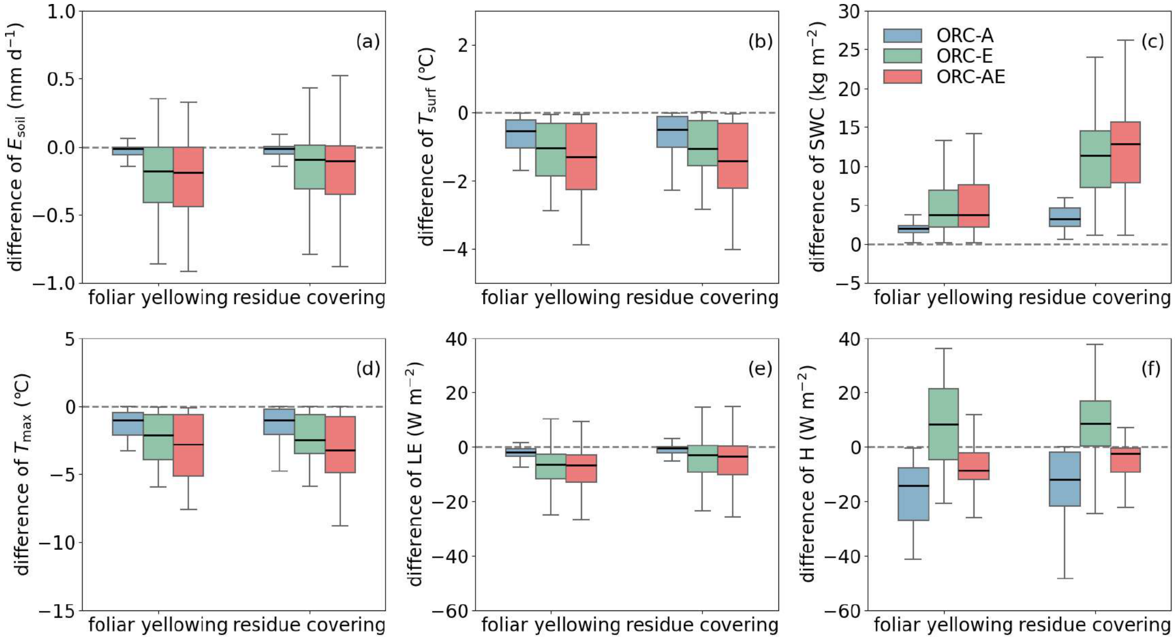

Figure 4. The average effect of model improvements for yellowing and residues cover on daily soil evaporation (E_{soil}), surface temperature (T_{surf}), the total soil water content up to 2 m (SWC), the maximum daily surface temperature (T_{max}), the latent heat flux (*LE*) and the sensible heat fluxes (H) across 12 sites. Shown are the simulated differences between three configurations of the refined model and old model: ORC-A represents the effect of the modified surface albedo (α_{surf}), ORC-E shows the effect of refined soil conductance (β_4) and surface roughness (Z_0), and ORC-AE indicates the effect of both modifications. The solid and dotted black lines within each box indicate the mean and median daily values across sites and timepoints, respectively. The box spans the interquartile range, covering the 25th percentile (lower bound) to the 75th percentile (upper bound). Black crossbars at the top and bottom represent the dataset's minimum and maximum values. The grey dotted vertical line in each plot represents zero on the y-axis.

ORC-AE leads to a statistically significant reduction in E_{soil} relative to ORC-D during foliar yellowing period, with an averaged decrease of $-0.18 \pm 0.08\,\mathrm{mm\,d^{-1}}$ (Fig. 4a). A slightly smaller but consistent reduction in E_{soil} ($-0.17 \pm 0.14\,\mathrm{mm\,d^{-1}}$) occurs during the residue covering period. Changes in β_4 and Z_0 (ORC-E) exert significant impacts on E_{soil} that are comparable in magnitude to those simulated by ORC-AE during both periods, whereas changes in α_{surf} alone (ORC-A) cause relatively minor and statistically insignificant reductions in E_{soil} for the same periods. The influence of crop residues on E_{soil} disappears within approximately 40 d after residue coverage (Figs. S6a and S7a in the Supplement).

The reduced E_{soil} in ORC-AE leads to a modest but not significant increase in SWC over 2 m soil depth during the residue covering period among all sites ($13.30 \pm 8.02\,\mathrm{kg\,m^{-2}}$) (Fig. 4c, Table S5). The combined effect is comparable to the sum of the individual contributions from α_{surf} (ORC-A) and from β_4 and Z_0 (ORC-E), suggesting an approximately additive effect. Although statistically insignificant, this weak water conservation signal persists toward the end of year, with gradual infiltration into deeper soil layers (Fig. S8 in the Supplement).

Incorporating changes in α_{surf}, β_4 and Z_0 in ORC-AE results in a statistically significant reduction in T_{surf} during foliar yellowing and residue covering periods with averaged cooling of -1.55 ± 0.93 and -1.90 ± 0.88 °C over all sites, respectively, relative to ORC-D simulation (Fig. 4b). The factorial simulation experiments show that this cooling effect is mainly driven by changes in E_{soil} and Z_0 (ORC-E), whereas increased α_{surf} alone produces a weaker and statistically insignificant T_{surf} reductions. Interaction among α_{surf}, β_4 and Z_0 (ORC-AE) lead to a dampened overall effect compared with the individual effects of these factors on T_{surf}. The reduction in T_{surf} gradually weakened over approximately 60 d as residue cover decreased (Figs. S6d and S7d).

3.3 The impact of improved surface albedo, surface roughness and soil conductance on latent and sensible heat flux

Relative to the ORC-D simulation, statistically significant changes in latent heat fluxes (*LE*) induced by modifications in surface albedo (α_{surf}), surface roughness (Z_0), and soil conductance (β_4) are detected across sites for ORC-AE, ORC-A, and ORC-E configurations ($p < 0.05$ in t test) (Table S5). Changes in sensible heat fluxes (H) are also statistically significant for ORC-AE and ORC-A, whereas modifi-

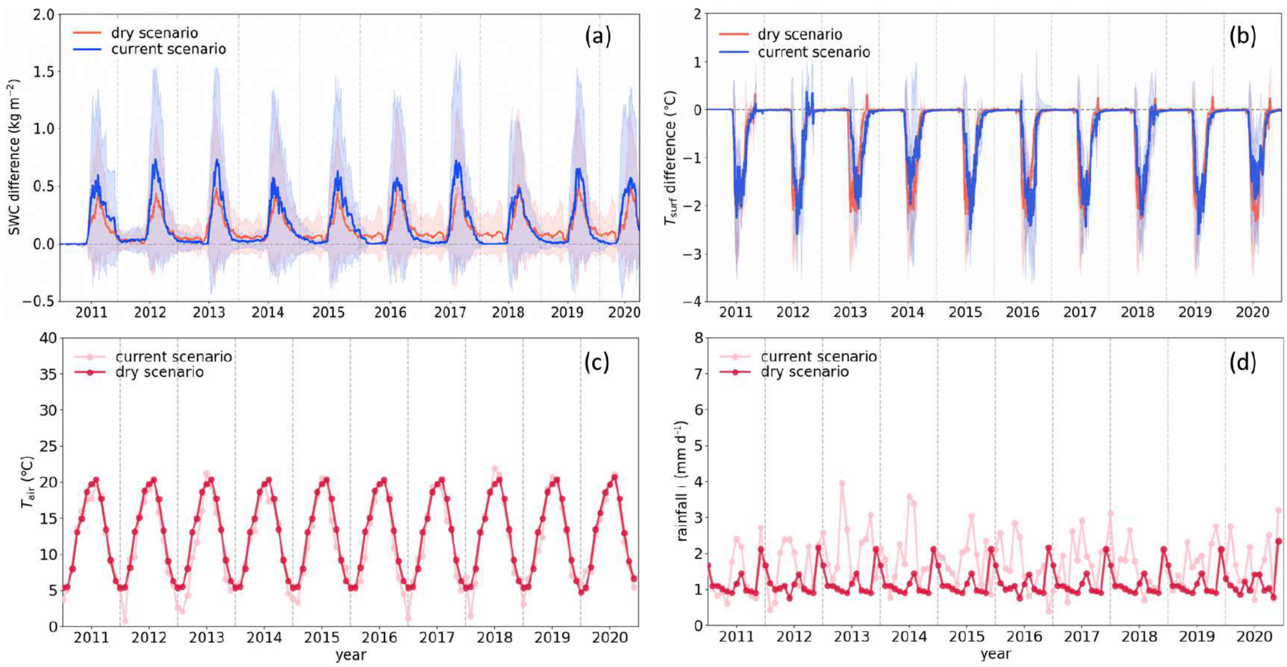

Figure 5. The 10-year cumulated effect of new parameterization of surface albedo (α_{surf}), surface roughness (Z_0) and soil conductance (β_4) on **(a)** soil water content (SWC) and **(b)** simulated daily soil temperature (T_{soil}) at 12.5 % soil depth under current and dry scenarios at six sites from 2011 to 2020. Monthly temperature and rainfall are obtained from the meteorological variables of 6-hourly 0.5° CRU-JRA product (v2.4), shown in **(c)** and **(d)**. Shown are differences between results from ORC-AE and ORC-D. ORC-AE represents the new model version with effects of the modified α_{surf} and the refined β_4 and Z_0, while ORC-D suggests the initial version of the model.

cations in Z_0 and β_4 alone (ORC-E) do not produce statistically significant changes in H ($p > 0.05$). This suggests that the modified model configurations capture systematic variations in surface water and energy exchanges when averaged across sites.

Modified α_{surf}, β_4 and Z_0 in ORC-AE leads to statistically significant reductions in LE during the foliar yellowing and residue covering periods, with the changes of -6.84 ± 1.41 and $-5.15 \pm 4.03\,\mathrm{W\,m^{-2}}$, respectively (Fig. 4e). This response is primarily controlled by changes in β_4 and Z_0, represented by comparable reductions in LE by ORC-E. While α_{surf} alone (ORC-A) plays a more limited role, the effect remains statistically significant. The corresponding changes in the H are also statistically significant and of similar magnitude to the changes in LE induced by the combined effect of α_{surf}, β_4 and Z_0 during the foliar yellowing and residue covering periods, with averaged decreases of -8.10 ± 4.18 and of $-7.44 \pm 3.98\,\mathrm{W\,m^{-2}}$, compared to the ORC-D simulation (Fig. 4f). In both periods, direct radiative effects associated with increased α_{surf} (ORC-A) contribute most strongly to the reduction in H, whereas changes in the surface–atmosphere energy exchange (ORC-E) leads only to a slight and statistically insignificant increase in H. Consistent with T_{surf} response, the influence of crop residues on H weakens over approximately 60 d of residue cover (Figs. S6c and S7c).

3.4 Effect of soil residues on soil water availability on multi-year timescale

The 10-year simulation under current climate shows a minor short-lived increase in SWC at the soil depth of 0.25 m (relative root depth of winter wheat in ORCHIDEE-CROP model) due to the presence of crop residues. Averaged across the simulation period and the six sites, total SWC is $0.24 \pm 0.60\,\mathrm{kg\,m^{-2}}$ (2.81 ± 6.15 %) higher than in the simulation without crop residues (Fig. 5a). No clear carry-over effect of SWC retention from one growing season to the next is observed at any site. This occurs because increased drainage losses compensated for reduced bare soil evaporation (Fig. S9 in the Supplement). Soil temperature (T_{soil}) at 0.25 m soil depth penetrable by winter wheat roots decreased by an average of -0.37 ± 0.77 °C (7.56 ± 5.96 %) over the 60 d of residue covering periods across sites, with no consistent temporal evolution during the 60 d residue covering periods over 10 years (Fig. 5b). The largest reduction in T_{soil} occurs shortly after harvest, coinciding with the largest increase in α_{surf} due to residue presence compared to simulation without residue effects.

In the dry scenario, the meteorological forcing corresponds to a single dry year that is repeatedly applied over the 10-year simulation. This idealized experiment is designed to explore the sustained response of the system under persistent dry conditions, rather than to represent future climatic conditions or interannual climate variability.

Under these conditions, the presence of crop residue shows a similar increase in SWC at 0.25 m soil depth under current climate, with an average increase of $0.23 \pm 0.53\,\mathrm{kg\,m^{-2}}$ ($3.01 \pm 5.97\,\%$) compared to simulations without residues (Fig. 5a).

Although no systematic temporal evolution is observed in near-surface SWC (at the soil depth of 0.25 m), deeper soil layers (50 % soil depth) exhibit a slight gradual increase of soil moisture over the simulation period (not shown) due to the sustained reduced E_{soil} which increases downward water transport. The decrease in E_{soil} by crop residues allows more water to remain in the soil, leaving more residual moisture available for the next growing season.

Average T_{soil} at 0.25 m soil depth decreases with a statistically significant trend by an average of $-0.42 \pm 0.80\,°\mathrm{C}$ ($-8.42 \pm 3.58\,\%$) over years (Fig. 5b), consistent with the sustained effects of residue-induced surface cooling.

3.5 Sensitivity of energy and water processes to parameters

Sensitivity analyses reveal pronounced nonlinear responses of land surface water and energy processes to variations in model parameters (Fig. S10 in the Supplement). For T_{surf}, k_1 exhibits the highest sensitivity, as it governs both the rate and maximum magnitude of the 15 d in surface albedo and consequently modulates available surface radiation during the residue covering period (Fig. S10a). A $\pm 30\,\%$ perturbation in k_1 induces 8.69 % and 30.78 % enhancements in surface cooling, respectively. This reflects a nonlinear response, as k_1 controls not only the rate of albedo increase but also the initial value of the subsequent decay phase (Sect. 2.3.2). Combined with the gradual decline in residue fraction over time, changes in k_1 modify the cumulative contribution of residue albedo to surface radiation, leading to enhanced cooling in both cases. In contrast, T_{surf} is only weakly affected by the hydrological parameter β_4 ($-4.46\,\%/+2.98\,\%$ change in surface cooling for $\pm 30\,\%$ variations), consistent with the scenario simulations (Fig. 4b). The parameter D_{up} also exerts only a limited influence on T_{surf} ($-8.35\,\%/+2.53\,\%$ change in cooling for $\pm 30\,\%$ variations).

For E_{soil}, β_4 is the dominant control (Fig. S10b). A decrease or increase in β_4 from the baseline by 30 % results in a 62.48 % reduction or 100.85 % increase in the decline of E_{soil}, respectively. The parameters k_1, k_4, and D_{up} also influence E_{soil}, with a $\pm 30\,\%$ variation leading to $-32.40\,\%/-35.53\,\%$, $-17.72\,\%/+22.35\,\%$, and $-29.49\,\%/-18.57\,\%$ changes, respectively.

For H, D_{up} exerts the strongest control, followed by k_1 and β_4 (Fig. S10c). Adjusting these parameters by $\pm 30\,\%$ alters H by $-10.53\,\%/+56.34\,\%$, $-42.55\,\%/+36.77\,\%$, and $-27.60\,\%/+27.33\,\%$, respectively. β_4 is also the most sensitive parameter controlling LE, reflecting the dependence of LE on E_{soil}. $\pm 30\,\%$ variations in β_4 yield $+89.78\,\%/-62.16\,\%$ changes in LE (Fig. S10d). In contrast, the strong sensitivity of E_{soil} to k_1 does not propagate to LE, with only $-2.66\,\%/+8.21\,\%$ changes observed under equivalent k_1 perturbations (Fig. S10c and d).

4 Discussion

4.1 Surface energy and land–atmosphere interaction jointly regulate surface temperature during foliar yellowing and residue covering periods

Foliar yellowing and residue coverage cool the surface across all sites by regulating the surface energy balance and redistributing net radiation to latent and sensible energy fluxes (Fig. 4a). Compared with the initial expectation that would dominate the impact of α_{surf}, the larger surface temperature (T_{surf}) decrease in ORC-E than that in ORC-A reveals that the cooling from the surface–atmosphere water–heat exchange due to modified soil conductance (β_4) and surface roughness (Z_0) drives the change in T_{surf}. Previous work indicated that no-tillage systems with residue coverage at the European scale cooled the surface by approximately 2 °C during hot summer days due to increased α_{surf} (Davin et al., 2014). Our simulations at site scale further highlight that the local changes in turbulent processes can exert a comparable control over T_{surf}, relying on different spatial scales, climate conditions, phenological stages and surface properties (McDermid et al., 2019).

While foliar yellowing and residue coverage induce an albedo-driven redistribution of surface energy budget across all 10 European sites, the interplay between available surface energy and the surface–atmosphere water–heat exchange causes substantial variation in the magnitude and duration of cooling. The increased Z_0 during winter wheat growth and residue covering periods enhances surface–atmosphere turbulent heat exchange, potentially promoting more efficient heat dissipation and surface cooling (Winckler et al., 2019; Meier et al., 2022). For example, when isolating the impact of increased Z_0 due to foliar yellowing and residue coverage (ORC-Z_0), both contribute more to the cooling impact than ORC-β_4 across all sites (Fig. S11a in the Supplement). However, the persistence of this surface cooling also depends on the hydrological fluxes between surface and atmosphere. Crop residues potentially warm the surface by decreasing soil evaporation (E_{soil}) (Hu et al., 2018). This effect can occur through reductions in β_4 caused by shielding the soil from direct solar radiation and wind (Fig. S11a), and by reducing near-surface wind speed and enhancing aerodynamic drag via increasing Z_0 (Figs. 4a and S11b). Similar to residue coverage, foliar yellowing has a comparable influence on E_{soil} due to the continuous coverage provided by winter wheat (Fig. 4a). The associated decline in transpiration, driven by reduced stomatal conductance under lower net radiation, may contribute to surface warming (not shown). Residue-induced suppression of E_{soil} during the residue covering period and radiation-induced decline in transpiration during foliar yellowing, both redirect energy partitioning from latent heat flux (*LE*) towards sensible heat flux (H), likely offsetting surface cooling (Fig. 4f) (Ramos et al., 2024).

4.2 Distinct controls on *LE* and *H* during foliar yellowing and residue covering periods

To isolate the drivers of turbulent flux changes during crop yellowing and residue cover periods, we analyzed results from two key model configurations: the surface–atmosphere interaction experiments (ORC-E) and the radiative forcing experiments (ORC-A). Our simulations revealed that the surface–atmosphere interactions (ORC-E) dominate the reduction in *LE* during both periods (Figs. 4e and S6b), with this effect jointly mediated by changes in β_4 and Z_0 (Fig. S11d), while α_{surf}-driven radiative impact is less important. In contrast, the reduced availability of surface energy with a higher albedo during crop yellowing and the residue cover period, together with the subsequently altered turbulent fluxes, contributed to a modest reduction in H during these periods due to their opposing effects (Figs. 4f and S6c). During this process, the enhanced H is primarily mediated by Z_0 (Fig. S11c).

The different underlying drivers behind changes in *LE* and H can be explained by the following: *LE* represents the energy needed for water vaporization and is therefore constrained by available energy and moisture transport efficiency (Chen et al., 2024). In contrast, H is driven by direct surface–atmosphere heat transfer via conduction and convection, governed by the land-air temperature gradient and turbulent heat exchange (Myhre et al., 2018). For example, we found that during the residue covering period, changes in β_4 and Z_0 (ORC-E) tend to increase H, while the albedo-induced reduction in net radiation (ORC-A) acts in the opposite direction by limiting the available energy for sensible heating (Fig. 4f). These results highlight that changes in *LE* and H are not controlled by a single mechanism but emerge from the combined and counteracting effects of radiative forcing and surface–atmosphere coupling. This finding is consistent with earlier findings pointing to a critical role of surface–atmosphere interactions in shaping energy partitioning and near-surface thermal dynamics (Koster et al., 2004; Seneviratne et al., 2010; Dare-Idowu et al., 2021; Denissen et al., 2022; Hsu and Dirmeyer, 2023).

The individual impacts of α_{surf} (ORC-A) and surface–atmosphere exchange (ORC-E) on the changes in *LE* and H differ from their combined effect of both (ORC-AE), especially during the residue covering period (Fig. 4). This indicates a strong nonlinear interaction between energy and water dynamics driven by crop residues (Hsu and Dirmeyer, 2021). For example, the decreased *LE* reduces H during the residue covering period by weakening near-surface turbulence, thereby producing a residual negative impact on H that could not be explained by ORC-A and ORC-E individually (Fig. 4f, Table S5). The complex feedback mechanisms between radiation partitioning and surface–atmosphere coupling require modelling approaches which take into account both interactions (Hsu and Dirmeyer, 2021, 2022).

It should be noted that in both periods, the averaged difference in surface energy fluxes (i.e. *LE* and H) between the new and old models across all sites are generally modest (Fig. 4e and f) and are of similar magnitudes to the model uncertainty (Table S5), which masks a substantial spatiotemporal variability in the effects of yellowed leaves and covered residues. Temporally, residue-induced albedo enhancement peaks within the first 15 d after harvest and weakens as residues decompose, causing short-lived but locally significant perturbations in water and heat fluxes (Figs. 3, S5 and S6). The residue impact on the water–heat processes persists for approximately one additional month after residue removal through tillage or natural decomposition (Fig. S7). Spatial variations in climate, soil properties, and management practices amplify local differences in residue effects. For example, we found that during the residue covering period, BE-Lon exhibits the largest mean relative decrease in *LE* in the new model compared to the old model (-27.42 ± 26.20 %), whereas the change at DE-Geb is minimal (5.73 ± 64.90 %). This contrast arises because the higher soil moisture and sandy texture at BE-Lon support greater evaporative fluxes, whereas the limited soil water and clay-rich soil at DE-Geb favor energy dissipation as sensible rather than latent heat (Dumont et al., 2024; Buysse et al., 2023). In addition, long-term simulations show the accumulated residue impact on heat budgets. The 10-year simulation under the dry scenario shows a low but statistically significant cooling trend, with a yearly average of -0.3 °C (Fig. 5). This demonstrates that even modest instantaneous flux changes can produce meaningful long-term surface cooling effects.

4.3 Implication for climate change mitigation and adaptation

With approximately 60 % of global croplands having higher T_{surf} than surrounding natural biome types, elevated temperatures, particularly during extreme heat and drought events, pose a major issue for crop yields and food security (Lobell et al., 2012; Hatfield and Prueger, 2015; Lesk et al., 2022; Chen et al., 2024). Our simulations across all sites suggest that residue coverage alleviates heat stress by significantly decreasing maximum surface temperature (T_{max}) during approximately 30 d residue covering period and for up to 50 d afterward (Figs. S6e and S7e). This result aligns with previous findings on the cooling effect of crop residues (Davin et al., 2014; Webber et al., 2018; Su et al., 2021). Reduced surface T_{max} after crop harvest mitigates heat stress on soil biota, providing a more favorable growing environment for subsequent crop cycles (Hatfield et al., 2015). Sustained temperatures above 30 °C can stress mesophilic soil microbes, inhibiting decomposition and nutrient cycling (Pietikäinen et al., 2005). Our simulations show that residue cover reduces $T_{\max}$ beyond 30 °C on 26 % of days during the residue period and 3.8 % of days afterward, underscoring its role in regulating soil thermal condition. This buffering effect modifies microbial activity and soil organic matter decomposition rates depending on local climatic and environmental conditions, thereby influencing greenhouse gas emissions from soil respiration (Knight et al., 2024).

The increase in H during residue covering period reveals an increased surface-air temperature gradient caused by reduced T_{surf}, possibly leading to warming of the lower atmosphere which cannot be quantified by the land surface model only (Figs. 4, S6c, and S7c). This shift in energy partitioning from LE to H, driven by reduced E_{soil} due to residue coverage, might mitigate surface warming while potentially intensifying regional heat stress. Consequently, it introduces uncertainty regarding the effectiveness of crop residues as a climate mitigation strategy. Notably, the use of fixed air temperature forcing data partially explains the increase in H because the constant air temperature ignores atmospheric feedback (Luyssaert et al., 2014). As a result, the climate mitigation potential of residue management remains uncertain, and its regional impact on energy partitioning cannot be fully quantified. It is essential to consider not only surface cooling but also changes in air temperature, as the latter is more directly linked to climate dynamics. A coupled simulation, feasible with ORCHIDEE-CROP, would be needed for future studies.

Soil water content (SWC) dynamics play a key role in regulating the land–atmosphere interactions, as the increase in surface soil SWC, as due to residue effects on roughness and soil resistance, can decrease H partitioning via promoting E_{soil} (Myhre et al., 2018). The 10-year simulations further highlight that residue coverage has the potential to increase SWC and thereby mitigate drought stress, particularly under drier conditions with fewer rainfall events (Figs. 5 and S9). In such condition, SWC remains high within the upper 1 m soil for extended periods of up to 3 months. An earlier review suggested that dry soil condition might result in soil compaction and reduced hydraulic conductivity (Singh et al., 2018). This limits infiltration and slow downward water percolation, which might hinder the underlying mechanism responsible for upper-soil SWC retention simulated by the ORCHIDEE-CROP model. Notably, soil texture modulates this effect. For example, rapid water infiltration into deeper layers in sandy soils with high drainage reduces surface SWC availability for cooling and plant uptake (Fatichi et al., 2020; Wankmüller et al., 2024), highlighting how soil hydraulics constrain residue efficacy. The sustained SWC also fosters soil biota activity (e.g., fungi, earthworms), which enhance soil structure through aggregate formation and organic matter decomposition (Li et al., 2009). Improved soil structure increases water-holding capacity, creating a positive feedback loop where residue-induced SWC retention supports biological activity, which in turn amplifies long-term moisture retention. This synergy reveals that residue effects on SWC persist beyond immediate rainfall events, particularly in water-limited systems.

External factors such as tillage timing and precipitation frequency also affect the biophysical impacts of crop residues (Konapala et al., 2020). Early tillage, as observed at the FR-Gri site in 2018 (3 weeks after harvest), retains more SWC in the topsoil and removes the residue cover, thereby temporarily enhancing E_{soil} and LE after the end of residue covering (Fig. S12 in the Supplement). The strong soil water retention capacity of the silt–loam soil at this site further contributed to this effect (Houot et al., 2000). This process underscores the importance of management practices in regulating the diverse hydrological and thermal effects of residue covering. Targeted strategies are also essential for optimising water use, particularly facing warmer and drier climates (Swain et al., 2025).

4.4 Uncertainty and Limitations

Despite improvements to the ORCHIDEE-CROP model in simulating crop albedo changes associated with foliar yellowing and crop residues, as well as their biophysical climate impacts, uncertainties and limitations remain.

α_{surf} shows the most consistent improvement across sites, reflecting its direct control by the new parameterizations for foliar yellowing and residue covering (Figs. 2 and S4a, b). However, degraded performance is observed at two sites (DE-Geb in 2014 and FR-Aur in 2019; Fig. S5a and c). At these sites, the refined configuration simulates higher α_{surf} during foliar yellowing and residue covering than those estimated from site radiometer measurements. Surface conditions shown by the site photos suggest that the discrepancy may be related to limitations in the spatial representativeness of point-scale observations, which is further investigated in Sect. S1.2 in the Supplement. T_{surf} also improves significantly, especially during the foliar yellowing period (Fig. S4c and d). In contrast, LE and H exhibit moderate improvement during the residue covering period and little to no improvement during the crop growth and foliar yellowing periods (Fig. S4e–g). This performance is expected, as LE and H during the growing season are primarily governed by transpiration processes that are not recalibrated in this study. During the residue covering period, remaining biases in LE and H likely arise from unrepresented processes associated with residue cover, such as water interception and retention by residues and soil hydraulic heterogeneity. Limitation in the representation of land–atmosphere coupling in ORCHIDEE also contributes to persistent uncertainties in simulated turbulent fluxes (Sect. 4.3).

The ORCHIDEE-CROP model exhibits biases in simulating water and energy fluxes, and the performance of the new model in reproducing water–energy fluxes does not improve relative to the previous version when evaluated against site-level measurements at six sites (Fig. S4). Both the new and old models overestimate LE and H during foliar yellowing periods, while underestimating LE and overestimating H during residue covering periods. This overestimation during foliar yellowing periods might come from excessively strong vegetation–atmosphere coupling for crops within ORCHIDEE itself compared with observation (Zhang et al., 2022c). Observations indicate that LE is higher during periods with residue coverage than during periods of bare soil exposure (Fig. S13 in the Supplement). However, it remains unclear to what extent the observed difference in LE is driven by differences in weather conditions rather than by the presence or absence of residues. One possible source of bias during the residue covering period may be the simplification of model parameters. In the present version of ORCHIDEE-CROP, the effects of crop residues on surface–atmosphere coupling are quantified by modulating β_4 and Z_0. Both variables are represented using uniform assumptions to balance model complexity against the scarcity of data available for parameterization. Specifically, the impact of residues on β_4 was represented using an initial reduction factor of 0.5 at the beginning of the residue covering (Sect. 2.3.3). The residue influence on Z_0 was prescribed using a fixed residue height (0.5 m), derived from the average of measurements across five winter-wheat sites (Sect. 2.3.4, Table S3). These parameter choices are applied uniformly across all sites and therefore cannot explicitly represent local variation in residue characteristics, soil properties, atmospheric conditions and management practices. As a result, the model is incapable of fully resolving site-specific residue impacts, which potentially contributes to the bias of simulated LE and H at certain sites.

The sensitivity analysis also highlights the uncertainties associated with parameter selection (Fig. S10). The β_4 and k_1 exert strong control over the spatiotemporal partitioning of available energy between LE and H. The use of fixed parameter values and limited calibration based on only a few sites inevitably contributes to model uncertainty and constrains the representation of local variability.

We manually adjusted the total conductance associated with soil evaporation, transpiration and interception in ORCHIDEE-CROP by scaling it with $1 + f_{\mathrm{soil}}$ during residue cover periods (Chapin et al., 2011). The simulations showed improved agreement with observed T_{surf}, LE and H (Fig. S14 in the Supplement), indicating that the net biophysical impact of residue cover enhanced surface–atmosphere water and heat exchanges despite inhibiting soil evaporation, which is not well described in the current model. A test of quantifying the residue impact on E_{soil} at 15 field experiments distributed globally showed that residue cover exceeding 80 % resulted in an approximately 20 %–30 % reduction in E_{soil} during the residue covering period (not shown). Therefore, the assumed 50 % initial decline in β_4 in the improved model (Eq. 16) might overestimate residue impacts, potentially explaining the lower E_{soil} and LE simulated across sites in the new model compared with both the initial model version and observations (Fig. S4).

While our modelling shows minor effects of crop residues on SWC, we did not account for effects such as changes in soil texture or organic matter content (Singh et al., 2018), which could improve soil water availability to crops. In addition, we did not account for interactions with other managements such as tillage, which are often co-applied. In summary, the present simulations are particularly well suited for assessing the biophysical impacts of residue cover on the surface energy balance, while the representation of soil–water responses remains an area requiring further model development and the corresponding results should therefore be considered with caution.

For example, specific hydrological processes impacted by crop residues were not accounted for in this study, such as water interception on the surface of residues, and uptake or release of water by residues (Kozak et al., 2007, Swella et al., 2015). Rainfall interception by residues alters both the timing and magnitude of soil–water inputs and enhances evaporation from residue surfaces, thereby modifying surface moisture conditions and heat exchange processes (Mitchell et al., 2012; Thapa et al., 2021). However, contrasting evaporation mechanisms operating in soil and residue layers introduce additional complexity into surface evaporation processes. The omission of these processes likely increases model uncertainty in biophysical simulations under variable rainfall conditions.

The input data used to drive the model introduces several structural uncertainties. First, while site-based meteorological forcing (e.g., air temperature, wind speed, humidity) provides high representativeness, meteorological observations and direct radiation measurements were unavailable at two ClieNFarm sites comprising six farms (UK-Rookery, UK-Winwick, UK-Allerton, BE-AH, BE-BM, and BE-LB; Table S2). For these sites, simulations were instead driven by the hourly 0.25° ERA-interim product and surface albedo was derived from Sentinel-2 observations. This substitution inevitably limits the ability of our model to reproduce site-specific water and energy dynamics. A comparison between satellite-derived albedo at 300 m spatial resolution and albedo calculated from shortwave radiation measurements representing only a few m^2 at eight sites reveals systematic differences (Fig. S15 in the Supplement). These differences are likely attributable to spatial scale mismatch, cloud screening effects, and surface heterogeneity, which together dampen albedo variability in the satellite product. While satellite-based albedo enables the inclusion of these six field sites, the substituted values introduce additional uncertainty in the simulated surface energy fluxes. Second, the bare soil albedo dataset used to estimate surface albedo carries uncertainties related to quality-restricted training samples (Yu et al., 2026). For example, the vegetation index thresholding used to identify bare soil may also include mixed surfaces containing crop residues, introducing biases into soil albedo retrievals. Also, the spatial aggregation from 300 m to 0.5° smoothes the field variability of bare soil albedo, reducing the reliability of the model simulation. Third, the incomplete representation of management practices in our model, including fertilizer and pesticide application as well as physical operations such as tillage, limits the model's capacity to reproduce observed variations in crop phenology, soil water content, and surface fluxes across years.

Based on these concerns, evaluating residue effects requires a context-specific approach that accounts for the interactions among climate, soil, and crop characteristics. Process-based land surface models provide an effective framework for such assessments across multiple scales, as they explicitly represent the coupled biophysical and ecological mechanisms controlling surface energy and water exchanges. This approach provides opportunities to guide residue management strategies under diverse environmental settings. Future model developments should incorporate explicit residue modules and site-specific parameterization to better capture spatial heterogeneity in residue impacts on energy and water fluxes. For example, integrating the canopy interception modules developed by crop models to ORCHIDEE-CROP is a good strategy to better represent the residue impact on the hydrological dynamics, such as CropSyst and RZWQM (Kozak et al., 2007). Moreover, an open-sourced global database derived from dedicated field trials monitoring energy exchange is required for parametrizing and evaluating these model developments.

5 Conclusion

In this study, we improved the simulation of winter wheat cultivar in the ORCHIDEE-CROP model by taking into account the impact of foliar yellowing and crop residues on water and energy balance of winter wheat cultivations based on observations from 10 cropland sites. The simulated surface energy budget and partitioning of latent and sensible heat fluxes show a cooling impact of residues and crop yellowing. A complex interplay between radiative and turbulent processes controls the strength of these effects. The improved ORCHIDEE-CROP model, which includes representations of land surface albedo, surface roughness, and soil conductance for residue covering, provides a valuable tool for quantifying biophysical impacts and guiding localized residue management strategies from regional to global scales. Future model developments should refine the representation of crop residue effects on soil physio–chemical properties and interactions with management practices such as tillage in order to improve simulations of plant water availability. By identifying optimal residue management practices, this approach can contribute to sustainable agriculture and support policy development in the context of climate warming.

Code and data availability. The model code used in this study is archived at https://doi.org/10.5281/zenodo.15230286 (Yu and Su, 2025). All the data and the codes for data analysis and figure creation are available at https://doi.org/10.5281/zenodo.15234443 (Yu, 2025a). All data used in this study are publicly available. The original ecosystem flux data at available sites can be derived from the Integrated Carbon Observation System (ICOS) Data Portal at https://data.icos-cp.eu/ (last access: 11 May 2024). The MODIS LAI data (MCD15A3H) can be downloaded from Land Processes Distributed Active Archive Center (https://lpdaac.usgs.gov/products/mcd15a3hv006/, last access: 13 February 2026, DOI: https://doi.org/10.5067/MODIS/MCD15A3H.006, Myneni et al., 2015). The MODIS aerosol product (MO(Y)D04_L2) can be downloaded from Level-1 and Atmosphere Archive & Distribution System.

Distributed Active Archive Center (https://ladsweb.modaps.eosdis.nasa.gov/, last access: 13 February 2026, DOI: https://doi.org/10.5067/MODIS/MOD04_L2.061, Levy et al., 2015). The Sentinel-2 bare soil albedo datasets can be downloaded from https://doi.org/10.5281/zenodo.15271053 (Yu, 2025b).

Supplement. The supplement related to this article is available online at https://doi.org/10.5194/gmd-19-7217-2026-supplement.

Author contributions. DG, YS, RL, and PC conceptualized and designed the study. KY modified and implemented the model, conducted formal analysis of the results, and led the writing of the original draft with contributions from all co-authors. AP and MC contributed data curation by providing management information from ClieNFarm sites. All authors participated in reviewing, editing, and finalizing the manuscript.

Competing interests. The contact author has declared that none of the authors has any competing interests.

Acknowledgements. The authors gratefully acknowledge the ClieNFarm project partners for providing spatial datasets (shapefiles) and detailed management practice records for winter wheat fields within their agricultural sites. We also extend our thanks to the ORCHIDEE model development team for their technical support and expertise during the model implementation process.

Financial support. This project has received fundings from the ClieNFarms project, which is funded by the European Union's

Horizon 2020 research and innovation programme (Grant Agreement ID: 101036822), and the French government under the ANR "Investissements d'avenir" program (reference: CLAND ANR-16-CONV-0003).

Review statement. This paper was edited by Nathaniel Chaney and reviewed by three anonymous referees.

References

Arora, V. K., Seiler, C., Wang, L., and Kou-Giesbrecht, S.: Towards an ensemble-based evaluation of land surface models in light of uncertain forcings and observations, Biogeosciences, 20, 1313–1355, https://doi.org/10.5194/bg-20-1313-2023, 2023.

Bernhofer, C., Eichelmann, U., Gruenwald, T., Hehn, M., Mauder, M., Moderow, U., and Prasse, H.: ETC L2 ARCHIVE from Klingenberg, 2004–2025, ICOS RI, https://hdl.handle.net/11676/gDoAlPK25ObbnSEhWZLL7y08 (last access: 27 July 2026), 2026,

Brisson, N., Gary, C., Justes, E., Roche, R., Mary, B., Ripoche, D., Zimmer, D., Sierra, J., Bertuzzi, P., Burger, P., Bussière, F., Cabidoche, Y. M., Cellier, P., Debaeke, P., Gaudillère, J. P., Hénault, C., Maraux, F., Seguin, B., and Sinoquet, H.: An overview of the crop model STICS, Eur. J. Agron., 18, 309–332, https://doi.org/10.1016/S1161-0301(02)00110-7, 2003.

Brümmer, C., Delorme, J., and Schrader, F.: ETC L2 ARCHIVE, Gebesee, 31 December 2019–31 December 2022, ICOS RI, https://hdl.handle.net/11676/HvHTkafa7I1hEIJn9f2ZOLB3 (last access: 27 July 2026), 2023.

Brut, A., Tallec, T., Granouillac, F., Zawilski, B., Claverie, N., Lemaire, B., and Ceschia, E.: ETC L2 ARCHIVE from Lamasquere, 2019-12-31–2023-12-31, ICOS RI, https://hdl.handle.net/11676/1_0Lbyl8AYSVncl5LYHMRFuG (last access: 27 July 2026), 2024.

Buysse, P., Depuydt, J., and Loubet, B.: ETC L2 ARCHIVE, Grignon, 31 DEcember 2022–30 September 2023, ICOS RI, https://hdl.handle.net/11676/26mBvWRW3gRwhfpCL4u9qysW (last access: 27 July 2026), 2023.

Campoy, A., Ducharne, A., Chéruy, F., Hourdin, F., Polcher, J., and Dupont, J. C.: Response of land surface fluxes and precipitation to different soil bottom hydrological conditions in a general circulation model, J. Geophys. Res.-Atmos., 118, 10725–10739, https://doi.org/10.1002/jgrd.50627, 2013.

Carbone, R. and Armstrong, J. S.: Evaluation of extrapolative forecasting methods: Results of a survey of academicians and practitioners, http://repository.upenn.edu/marketing_papers/80 (last access: 13 February 2026), 1982.

Chapin, F. S., Chapin, M. C., Matson, P. A., and Vitousek, P.: Principles of Terrestrial Ecosystem Ecology, Springer, New York, https://doi.org/10.1007/978-1-4419-9504-9, 2011.

Chen, C., Li, Y., Wang, X., Luo, X., Li, Y., Cheng, Y., and Zhu, Z.: Biophysical effects of croplands on land surface temperature, Nat. Commun., 15, 10901, https://doi.org/10.1038/s41467-024-55319-2, 2024.

Costa, M. H., Yanagi, S. N. M., Souza, P. J. O. P., Ribeiro, A., and Rocha, E. J. P.: Climate change in Amazonia caused by soybean cropland expansion, as compared to caused by pastureland expansion, Geophys. Res. Lett., 34, L07706, https://doi.org/10.1029/2007GL029271, 2007.

Dalgliesh, N., Hochman, Z., Huth, N., and Holzworth, D.: Field protocol to APSoil characterisations, version 4, CSIRO, Canberra, Australia, https://doi.org/10.4225/08/58542c1093a80, 2016.

Dare-Idowu, O., Brut, A., Cuxart, J., Tallec, T., Rivalland, V., Zawilski, B., Ceschia, E., and Jarlan, L.: Surface energy balance and flux partitioning of annual crops in southwestern France, Agr. Forest Meteorol., 308–309, 108529, https://doi.org/10.1016/j.agrformet.2021.108529, 2021.

Davin, E. L., Seneviratne, S. I., Ciais, P., Olioso, A., and Wang, T.: Preferential cooling of hot extremes from cropland albedo management, P. Natl. Acad. Sci. USA, 111, 9757–9761, https://doi.org/10.1073/pnas.1317323111, 2014.

de Rosnay, P., Polcher, J., Bruen, M., and Laval, K.: Impact of a physically based soil water flow and soil-plant interaction representation for modeling large-scale land surface processes, J. Geophys. Res., 107, https://doi.org/10.1029/2001JD000634, 2002.

Denissen, J. M. C., Teuling, A. J., Pitman, A. J., Koirala, S., Migliavacca, M., Li, W., Reichstein, M., Winkler, A. J., Zhan, C., and Orth, R.: Widespread shift from ecosystem energy to water limitation with climate change, Nat. Clim. Change, 12, 677–684, https://doi.org/10.1038/s41558-022-01403-8, 2022.

Drewry, D. T., Kumar, P., and Long, S. P.: Simultaneous improvement in productivity, water use, and albedo through crop structural modification, Glob. Change Biol., 20, 1955–1967, https://doi.org/10.1111/gcb.12567, 2014.

Ducoudré, N. I., Laval, K., and Perrier, A.: SECHIBA, a new set of parameterizations of the hydrologic exchanges at the land-atmosphere interface within the LMD atmospheric general circulation model, J. Climate, 6, 248–273, https://doi.org/10.1175/1520-0442(1993)006<0248:SANSOP>2.0.CO;2, 1993.

Dumont, B., Heinesch, B., Bodson, B., Bogaerts, G., Chopin, H., De Ligne, A., Demoulin, L., Douxfils, B., Engelmann, T., Faurès, A., Longdoz, B., Manise, T., Orgun, A., Piret, A., and Thyrion, T.: ETC L2 ARCHIVE from Lonzee, 2017-01-01–2024-09-01, ICOS RI, https://hdl.handle.net/11676/CiZeT-H6TJ4OtO9ke7UcBdhb (last access: 27 July 2026), 2024.

Fatichi, S., Or, D., Walko, R., Vereecken, H., Young, M. H., Ghezzehei, T. A., Hengl, T., Kollet, S., Agam, N., and Avissar, R.: Soil structure is an important omission in Earth System Models, Nat. Commun., 11, 522, https://doi.org/10.1038/s41467-020-14411-z, 2020.

Féret, J.-B., Gitelson, A. A., Noble, S. D., and Jacquemoud, S.: PROSPECT-D: Towards modeling leaf optical properties through a complete lifecycle, Remote Sens. Environ., 193, 204–221, https://doi.org/10.1016/j.rse.2017.03.004, 2017.

Fisher, J. B., Huntzinger, D. N., Schwalm, C. R., and Sitch, S.: Modeling the terrestrial biosphere, Annu. Rev. Environ. Resour., 39, 91-123, https://doi.org/10.1146/annurev-environ-012913-093456, 2014.

Fisher, R. A. and Koven, C. D.: Perspectives on the future of land surface models and the challenges of representing complex terrestrial systems, J. Adv. Model. Earth Sy., 12, e2018MS001453, https://doi.org/10.1029/2018MS001453, 2020.

Hatfield, J. L. and Prueger, J. H.: Temperature extremes: effect on plant growth and development, Weather Clim. Extremes, 10, 4–10, https://doi.org/10.1016/j.wace.2015.08.001, 2015.

Hoogenboom, G., Porter, C. H., Shelia, V., Boote, K. J., Singh, U., Pavan, W., Oliveira, F. A. A., Moreno-Cadena, L. P., Ferreira, T. B., White, J. W., Lizaso, J. I., Pequeno, D. N. L., Kimball, B. A., Alderman, P. D., Thorp, K. R., Cuadra, S. V., Vianna, M. S., Villalobos, F. J., Batchelor, W. D., Asseng, S., Jones, M. R., Hopf, A., Dias, H. B., Jintrawet, A., Jaikla, R., Memic, E., Hunt, L. A., and Jones, J. W.: Decision Support System for Agrotechnology Transfer (DSSAT) Version 4.8.5, DSSAT Foundation, Gainesville, Florida, USA, https://www.DSSAT.net (last access: 27 July 2026), 2024.

Horton, P., Ruban, A. V., and Walters, R. G.: Regulation of light harvesting in green plants, Annu. Rev. Plant Phys., 47, 655-684, https://doi.org/10.1146/annurev.arplant.47.1.655, 1996.

Houot, S., Topp, E., Yassir, A., and Soulas, G.: Dependence of accelerated degradation of atrazine on soil pH in French and Canadian soils, Soil Biol. Biochem., 32, 615–625, https://doi.org/10.1016/S0038-0717(99)00188-1, 2000.

Hsu, H. and Dirmeyer, P. A.: Nonlinearity and multivariate dependencies in the terrestrial leg of land-atmosphere coupling, Water Resour. Res., 57, e2020WR028179, https://doi.org/10.1029/2020WR028179, 2021.

Hsu, H. and Dirmeyer, P. A.: Deconstructing the soil moisture-latent heat flux relationship: The range of coupling regimes experienced and the presence of nonlinearity within the sensitive regime, J. Hydrometeorol., 23, 1041-1057, https://doi.org/10.1175/JHM-D-21-0224.1, 2022.

Hsu, H. and Dirmeyer, P. A.: Soil moisture-evaporation coupling shifts into new gears under increasing CO_2, Nat. Commun., 14, 1162, https://doi.org/10.1038/s41467-023-36794-5, 2023.

Hu, C., Zheng, C., Sadras, V. O., Ding, M., Yang, X., and Zhang, S.: Effect of straw mulch and seeding rate on the harvest index, yield, and water use efficiency of winter wheat, Sci. Rep., 8, 8167, https://doi.org/10.1038/s41598-018-26615-x, 2018.

IPCC: Climate Change 2014: Synthesis Report, Contribution of Working Groups I, II and III to the Fifth Assessment Report of the Intergovernmental Panel on Climate Change, IPCC, Geneva, Switzerland, 151 pp., https://www.ipcc.ch/report/ar5/syr/ (last access: 27 July 2026), 2014.

Jacobs, A. F. G. and van Pul, W. A. J.: Seasonal changes in the albedo of a maize crop during two seasons, Agr. Forest Meteorol., 49, 351–360, https://doi.org/10.1016/0168-1923(90)90006-R, 1990.

Knight, C. G., Nicolitch, O., Griffiths, R. I., Goodall, T., Jones, B., Weser, C., Langridge, H., Davison, J., Dellavalle, A., Eisenhauer, N., Gongalsky, K. B., Hector, A., Jardine, E., Kardol, P., Maestre, F. T., Schädler, M., Semchenko, M., Stevens, C., Tsiafouli, M. A., Vilhelmsson, O., Wanek, W., and de Vries, F. T.: Soil microbiomes show consistent and predictable responses to extreme events, Nature, 636, 690–696, https://doi.org/10.1038/s41586-024-08185-3, 2024.

Konapala, G., Mishra, A. K., Wada, Y., and Mann, M. E.: Climate change will affect global water availability through compounding changes in seasonal precipitation and evaporation, Nat. Commun., 11, 3044, https://doi.org/10.1038/s41467-020-16757-w, 2020.

Koster, R. D., Dirmeyer, P. A., Guo, Z., Bonan, G., Chan, E., Cox, P., Gordon, C. T., Kanae, S., Kowalczyk, E., Lawrence, D., Liu, P., Lu, C.-H., Malyshev, S., McAvaney, B., Mitchell, K., Mocko, D., Oki, T., Oleson, K., Pitman, A., Sud, Y. C., Taylor, C. M., Verseghy, D., Vasic, R., Xue, Y., and Yamada, T.: Regions of strong coupling between soil moisture and precipitation, Science, 305, 1138–1140, https://doi.org/10.1126/science.1100217, 2004.

Kozak, J. A., Ahuja, L. R., Green, T. R., and Ma, L.: Modelling crop canopy and residue rainfall interception effects on soil hydrological components for semi-arid agriculture, Hydrol. Process., 21, 229–241, https://doi.org/10.1002/hyp.6235, 2007.

Krinner, G., Viovy, N., de Noblet-Ducoudré, N., Ogée, J., Polcher, J., Friedlingstein, P., Ciais, P., Sitch, S., and Prentice, I. C.: A dynamic global vegetation model for studies of the coupled atmosphere-biosphere system, Global Biogeochem. Cy., 19, GB1015, https://doi.org/10.1029/2003GB002199, 2005.

Lascano, R. J. and Baumhardt, R. L.: Effects of crop residue on soil and plant water evaporation in a dryland cotton system, Theor. Appl. Climatol., 54, 69–84, https://doi.org/10.1007/BF00863560, 1996.

Lei, C., Chen, J., Ibáñez, I., Sciusco, P., Shirkey, G., Lei, M., Reich, P., and Robertson, G. P.: Albedo of crops as a nature-based climate solution to global warming, Environ. Res. Lett., 19, 084032, https://doi.org/10.1088/1748-9326/ad5fa2, 2024.

Lesk, C., Anderson, W., Rigden, A., Coast, O., Jägermeyr, J., McDermid, S., Davis, K. F., and Konar, M.: Compound heat and moisture extreme impacts on global crop yields under climate change, Nat. Rev. Earth Environ., 3, 872–889, https://doi.org/10.1038/s43017-022-00368-8, 2022.

Levy, R., Hsu, C., et al.: MODIS Atmosphere L2 Aerosol Product. NASA MODIS Adaptive Processing System, Goddard Space Flight Center, USA [data set], https://doi.org/10.5067/MODIS/MOD04_L2.061, 2015.

Li, S.-X., Wang, Z.-H., Malhi, S. S., Li, S.-Q., Gao, Y.-J., and Tian, X.-H.: Nutrient and water management effects on crop production, and nutrient and water use efficiency in dryland areas of China, Adv. Agron., 102, 223–265, https://doi.org/10.1016/S0065-2113(09)01007-4, 2009.

Lin, X. W., Wu, S., Chen, B., Lin, Z., Yan, Z., Chen, X., Yin, G., You, D., Wen, J., Liu, Q., Xiao, Q., Liu, Q., and Lafortezza, R.: Estimating 10-m land surface albedo from Sentinel-2 satellite observations using a direct estimation approach with Google Earth Engine, ISPRS J. Photogramm., 194, 1–20, https://doi.org/10.1016/j.isprsjprs.2022.09.016, 2023.

Lobell, D., Sibley, A., and Ortiz-Monasterio, J. I.: Extreme heat effects on wheat senescence in India, Nat. Clim. Change, 2, 186–189, https://doi.org/10.1038/nclimate1356, 2012.

Luyssaert, S., Jammet, M., Stoy, P. C., Estel, S., Pongratz, J., Ceschia, E., Churkina, G., Don, A., Erb, K.-H., Ferlicoq, M., Gielen, B., Grünwald, T., Houghton, R. A., Klumpp, K., Knohl, A., Kolb, T., Kuemmerle, T., Laurila, T., Lohila, A., Loustau, D., McGrath, M. J., Meyfroidt, P., Moors, E. J., Naudts, K., Novick, K., Otto, J., Pilegaard, K., Pio, C. A., Rambal, S., Rebmann, C., Ryder, J., Suyker, A. E., Varlagin, A., Wattenbach, M., and Dolman, A. J.: Land management and land-cover change have impacts of similar magnitude on surface temperature, Nat. Clim. Change, 4, 389–393, https://doi.org/10.1038/nclimate2196, 2014.

MacBean, N., Scott, R. L., Biederman, J. A., Ottlé, C., Vuichard, N., Ducharne, A., Kolb, T., Dore, S., Litvak, M., and Moore, D. J. P.: Testing water fluxes and storage from two hydrology configurations within the ORCHIDEE land surface model across US semi-arid sites, Hydrol. Earth Syst. Sci., 24, 5203–5230, https://doi.org/10.5194/hess-24-5203-2020, 2020.

McDermid, S. S., Mearns, L. O., and Ruane, A. C.: Representing agriculture in Earth System Models: Approaches and priorities for development, J. Adv. Model. Earth Sy., 9, 2230–2265, https://doi.org/10.1002/2016MS000749, 2017.

McDermid, S. S., Montes, C., Cook, B. I., Puma, M. J., and Kiang, N. Y.: The sensitivity of land-atmosphere coupling to modern agriculture in the Northern Midlatitudes, J. Climate, 32, 465–484, https://doi.org/10.1175/JCLI-D-17-0799.1, 2019.

McMaster, G. S., Aiken, R. M., and Nielsen, D. C.: Optimizing wheat harvest cutting height for harvest efficiency and soil and water conservation, Agron. J., 92, 1104–1108, https://doi.org/10.2134/agronj2000.9261104x, 2000.

Meier, R., Davin, E. L., Bonan, G. B., Lawrence, D. M., Hu, X., Duveiller, G., Prigent, C., and Seneviratne, S. I.: Impacts of a revised surface roughness parameterization in the Community Land Model 5.1, Geosci. Model Dev., 15, 2365–2393, https://doi.org/10.5194/gmd-15-2365-2022, 2022.

Mitchell, J. P., Singh, P. N., Wallender, W. W., Munk, D. S., Wroble, J. F., Horwath, W. R., and Scow, K. M.: No-tillage and high-residue practices reduce soil water evaporation, Calif. Agr., 66, https://doi.org/10.3733/ca.v066n02p55, 2012.

Myhre, G., Samset, B. H., Hodnebrog, Ø., Andrews, T., Boucher, O., Faluvegi, G., Fläschner, D., Forster, P. M., Kasoar, M., Kharin, V., Kirkevåg, A., Lamarque, J.-F., Olivié, D., Richardson, T. B., Shawki, D., Shindell, D., Shine, K. P., Stjern, C. W., Takemura, T., and Voulgarakis, A.: Sensible heat has significantly affected the global hydrological cycle over the historical period, Nat. Commun., 9, 1922, https://doi.org/10.1038/s41467-018-04307-4, 2018.

Myneni, R., Knyazikhin, Y., and Park, T.: MCD15A3H MODIS/Terra+Aqua Leaf Area Index/FPAR 4-day L4 Global 500m SIN Grid V006, NASA EOSDIS Land Processes DAAC [data set], https://doi.org/10.5067/MODIS/MCD15A3H.006, 2015.

Pastorello, G., Trotta, C., Canfora, E., et al.: The FLUXNET2015 dataset and the ONEFlux processing pipeline for eddy covariance data, Sci. Data, 7, 225, https://doi.org/10.1038/s41597-020-0534-3, 2020.

Pietikäinen, J., Pettersson, M., and Bååth, E.: Comparison of temperature effects on soil respiration and bacterial and fungal growth rates, FEMS Microbiol. Ecol., 52, 49–58, https://doi.org/10.1016/j.femsec.2004.10.002, 2005.

Pique, G., Carrer, D., Lugato, E., Fieuzal, R., Garisoain, R., and Ceschia, E.: About the assessment of cover crop albedo potential cooling effect: risk of the darkening feedback loop effects, Remote Sens., 15, 3231, https://doi.org/10.3390/rs15133231, 2023.

Raes, D., Steduto, P., Hsiao, T. C., and Fereres, E.: AquaCrop reference manual: Chapter 2–Calculation procedures (Version 7.0), Food and Agriculture Organization of the United Nations, http://www.fao.org/aquacrop (last access: 24 February 2026), 2022.

Ramos, T. B., Darouich, H., and Pereira, L. S.: Mulching effects on soil evaporation, crop evapotranspiration and crop coefficients: a review aimed at improved irrigation management, Irrig. Sci., 42, 525–539, https://doi.org/10.1007/s00271-024-00924-8, 2024.

Richards, L. A.: Capillary conduction of liquids through porous mediums, Physics, 1, 318–333, https://doi.org/10.1063/1.1745010, 1931.

Şerban, G., Cotfas, D. T., and Cotfas, P. A.: Significant differences in crop albedo among Romanian winter wheat cultivars, Rom. Agric. Res., 28, 1–7, 2011.

Schmidt, M., Bagheri, S., Becker, N., Dolfus, D., Esser, O., Graf, A., Haustein, A., Kettler, M., Kummer, S., and Mattes, J.: ETC L2 ARCHIVE from Selhausen Juelich, 2019-2024, ICOS RI, https://hdl.handle.net/11676/bhnFE28dct4cSz18cBl14rvb, 2025.

Seneviratne, S. I., Corti, T., Davin, E. L., Hirschi, M., Jaeger, E. B., Lehner, I., Orlowsky, B., and Teuling, A. J.: Investigating soil moisture-climate interactions in a changing climate: A review, Earth-Sci. Rev., 99, 125–161, https://doi.org/10.1016/j.earscirev.2010.02.004, 2010.

Seneviratne, S. I., Phipps, S. J., Pitman, A. J., Hirsch, A. L., Davin, E. L., Donat, M. G., Hirschi, M., Lenton, A., Wilhelm, M., and Kravitz, B.: Land radiative management as contributor to regional-scale climate adaptation and mitigation, Nat. Geosci., 11, 88–96, https://doi.org/10.1038/s41561-017-0057-5, 2018.

Sieber, P., Böhme, S., Ericsson, N., and Hansson, P.-A.: Albedo on cropland: Field-scale effects of current agricultural practices in Northern Europe, Agr. Forest Meteorol., 321, 108978, https://doi.org/10.1016/j.agrformet.2022.108978, 2022.

Simão, L. M., Easterly, A. C., Kruger, G. R., and Creech, C. F.: Winter wheat residue impact on soil water storage and subsequent corn yield, Agron. J., 113, 276–286, https://doi.org/10.1002/agj2.20459, 2021.

Singh, R., Serawat, M., Singh, A., and Babli, A.: Effect of tillage and crop residue management on soil physical properties, J. Soil. Salin. Water Qual., 10, 200–206, 2018.

Stephens, G. L., O'Brien, D., Webster, P. J., Pilewski, P., Kato, S., and Li, J.-L.: The albedo of Earth, Rev. Geophys., 53, 141–163, https://doi.org/10.1002/2014RG000449, 2015.

Su, Y., Gabrielle, B., and Makowski, D.: The impact of climate change on the productivity of conservation agriculture, Nat. Clim. Change, 11, 628–633, https://doi.org/10.1038/s41558-021-01075-w, 2021.

Su, Y., Lauerwald, R., Makowski, D., Viovy, N., Guilpart, N., Zhu, P., Gabrielle, B., and Ciais, P.: Future warming increases the chance of success of maize-wheat double cropping in Europe, Eur. J. Agron., 170, 127723, https://doi.org/10.1016/j.eja.2025.127723, 2025.

Swain, D. L., Prein, A. F., Abatzoglou, J. T., Albano, C. M., Brunner, M., Diffenbaugh, N. S., Singh, D., Skinner, C. B., and Touma, D.: Hydroclimate volatility on a warming Earth, Nat. Rev. Earth Environ., 6, 35–50, https://doi.org/10.1038/s43017-024-00624-z, 2025.

Swella, G. B., Ward, P. R., Siddique, K. H. M., and Flower, K. C.: Combinations of tall standing and horizontal residue affect soil water dynamics in rainfed conservation agriculture systems, Soil Till. Res., 147, 30–38, https://doi.org/10.1016/j.still.2014.11.004, 2015.

Tallec, T., Ceschia, E., Granouillac, F., Claverie, N., Zawilski, B., Brut, A., Lemaire, B., and Gibrin, H.: ETC L2 ARCHIVE from Aurade, 2019–2025, ICOS RI, https://hdl.handle.net/11676/

E4Xm_4CfgdmdEFoni2AjKk4K (last access: 27 July 2026), 2026.

Thapa, R., Tully, K. L., Cabrera, M., Dann, C., Schomberg, H. H., Timlin, D., Gaskin, J., Reberg-Horton, C., and Mirsky, S. B.: Cover crop residue moisture content controls diurnal variations in surface residue decomposition, Agr. Forest Meteorol., 308–309, 108537, https://doi.org/10.1016/j.agrformet.2021.108537, 2021.

Timlin, D., Paff, K., and Han, E.: The role of crop simulation modeling in assessing potential climate change impacts, Agrosyst. Geosci. Environ., 7, e20453, https://doi.org/10.1002/agg2.20453, 2024.

Unger, P. W. and Parker, J. J.: Residue placement effects on decomposition, evaporation, and soil moisture distribution, Agron. J., 60, 469–472, https://doi.org/10.2134/agronj1968.00021962006000050008x, 1968.

Velička, R., and Raudonius, S.: The influence of crop residue type on their decomposition rate in the soil: a litterbag study, Žemdirbystė, 99, 227–236, https://www.scopus.com/pages/publications/84867158516 (last access: 4 August 2026), 2012.

Vuichard, N. and Papale, D.: Filling the gaps in meteorological continuous data measured at FLUXNET sites with ERA-Interim reanalysis, Earth Syst. Sci. Data, 7, 157–171, https://doi.org/10.5194/essd-7-157-2015, 2015.

Wankmüller, F. J. P., Delval, L., Lehmann, P., Baur, M. J., Cecere, A., Wolf, S., Or, D., Javaux, M., and Carminati, A.: Global influence of soil texture on ecosystem water limitation, Nature, 635, 631–638, https://doi.org/10.1038/s41586-024-08089-2, 2024.

Winckler, J., Reick, C. H., Bright, R. M., and Pongratz, J.: Importance of surface roughness for the local biogeophysical effects of deforestation, J. Geophys. Res.-Atmos., 124, 8605–8618, https://doi.org/10.1029/2018JD030127, 2019.

Webber, H., Ewert, F., Olesen, J. E., Müller, C., Fronzek, S., Ruane, A. C., Bourgault, M., Martre, P., Ababaei, B., Bindi, M., Ferrise, R., Finger, R., Fodor, N., Gabaldón-Leal, C., Gaiser, T., Jabloun, M., Kersebaum, K.-C., Lizaso, J. I., Lorite, I. J., Manceau, L., Moriondo, M., Nendel, C., Rodríguez, A., Ruiz-Ramos, M., Semenov, M. A., Siebert, S., Stella, T., Stratonovitch, P., Trombi, G., and Wallach, D.: Diverging importance of drought stress for maize and winter wheat in Europe, Nat. Commun., 9, 4249, https://doi.org/10.1038/s41467-018-06525-2, 2018.

Wright, S.: Correlation and causation, J. Agric. Res., 20, 557–585, 1921.

Wu, X., Vuichard, N., Ciais, P., Viovy, N., de Noblet-Ducoudré, N., Wang, X., Magliulo, V., Wattenbach, M., Vitale, L., Di Tommasi, P., Moors, E. J., Jans, W., Elbers, J., Ceschia, E., Tallec, T., Bernhofer, C., Grünwald, T., Moureaux, C., Manise, T., Ligne, A., Cellier, P., Loubet, B., Larmanou, E., and Ripoche, D.: ORCHIDEE-CROP (v0), a new process-based agro-land surface model: model description and evaluation over Europe, Geosci. Model Dev., 9, 857–873, https://doi.org/10.5194/gmd-9-857-2016, 2016.

Yu, K.: Datasets and processing codes for the work ⟨Resolving effects of leaf pigmentation changes and plant residue on the energy balance of winter wheat cultivation in the ORCHIDEE-CROP model⟩, Zenodo [data set], https://doi.org/10.5281/zenodo.15234443, 2025a.

Yu, K.: S2 bare soil albedo in European cropland regions used for "Resolving effects of leaf pigmentation changes and plant residue on the energy balance of winter wheat cultivation in the ORCHIDEE-CROP model", Zenodo [data set], https://doi.org/10.5281/zenodo.15271053, 2025b.

Yu, K., Su, Y., Ciais, P., Lauerwald, R., Ceschia, E., Makowski, D., Xu, Y., Abbessi, E., Bazzi, H., and Tallec, T.: Quantifying albedo impact and radiative forcing of management practices in European wheat cropping systems, Environ. Res. Lett., 19, 074042, https://doi.org/10.1088/1748-9326/ad5859, 2024.

Yu, K. and Su, Y.: ORCHIDEE-CROP v2.1: ORCHIDEE-CROP-RES (Version ORCHIDEE-CROP-V2.1), Zenodo [code], https://doi.org/10.5281/zenodo.15230286, 2025.

Zhang, X., Jiao, Z., Zhao, C., Qu, Y., Liu, Q., Zhang, H., Tong, Y., Wang, C., Li, S., Guo, J., Zhu, Z., Yin, S., and Cui, L.: Review of land surface albedo: variance characteristics, climate effect and management strategy, Remote Sens., 14, 1382, https://doi.org/10.3390/rs14061382, 2022a.

Zhang, Y. H., Yang, Y. B., Chen, C. L., Zhang, K. T., Jiang, H. Y., Cao, W. X., and Yan, Z. H.: Modeling leaf color dynamics of winter wheat in relation to growth stages and nitrogen rates, J. Integr. Agr., 21, 60–69, https://doi.org/10.1016/S2095-3119(20)63319-6, 2022b.

Zhang, Y., Narayanappa, D., Ciais, P., Li, W., Goll, D., Vuichard, N., De Kauwe, M. G., Li, L., and Maignan, F.: Evaluating the vegetation–atmosphere coupling strength of ORCHIDEE land surface model (v7266), Geosci. Model Dev., 15, 9111–9125, https://doi.org/10.5194/gmd-15-9111-2022, 2022c.

Zhao, Y., Mao, X., and Shukla, M. K.: A modified SWAP model for soil water and heat dynamics and seed-maize growth under film mulching, Agr. Forest Meteorol., 292–293, 108127, https://doi.org/10.1016/j.agrformet.2020.108127, 2020.